European Journal of Medicinal Chemistry 199 (2020) 112385

Contents lists available at ScienceDirect

European Journal of Medicinal Chemistry

journal homepage: http://www.elsevier.com/locate/ejmech

Research paper

Identification and optimization of piperine analogues as neuroprotective agents for the treatment of Parkinson's disease *via* the activation of Nrf2/keap1 pathway

Lun Wang [a, 1], Xiaoying Cai [a, 1], Mingsong Shi [a, 1], Linlin Xue [a], Shuang Kuang [a], Ruiling Xu [a], Wenyan Qi [a], Yan Li [b], Xu Ma [a], Ruijia Zhang [a], Feng Hong [a], Haoyu Ye [a, **], Lijuan Chen [a, *]

[a] State Key Laboratory of Biotherapy/Collaborative Innovation Center of Biotherapy and Cancer Center, West China Hospital of Sichuan University, Chengdu, 610041, China

[b] Department of Pharmaceutical and Biological Engineering, School of Chemical Engineering, Sichuan University, Chengdu, 610065, People's Republic of China

ARTICLE INFO

Article history:
Received 8 January 2020
Received in revised form
8 April 2020
Accepted 23 April 2020
Available online 5 May 2020

Keywords:
Parkinson's disease
Piperine analogues
Nrf2 activation
MPTP

ABSTRACT

Parkinson's disease (PD) is a slowly progressive and complex neurodegenerative disorder. Up to date, there are no approved drugs that could slow or reverse the neurodegenerative process of PD. Here, we reported the synthesis of series of piperine analogues and the evaluation of their neuroprotective effects against hydrogen peroxide (H_2O_2) induced damage in the neuron-like PC12 cells. Among these analogues, **3b** exhibited the most potent protection effect and its underlying mechanism was further investigated. Further results indicated that the ROS scavenging and cytoprotection effect of **3b** might be related to the Nrf2 activation and upregulation of related phase II antioxidant enzymes, such as HO-1 and NQO1. In *in vivo* study, oral administration (100 mg/kg) of **3b** significantly attenuated PD-associated behavioral deficits in a 1-methyl-4-phenyl-1,2,3,6-tetrahydropyridine (MPTP)-induced mouse model of PD and protected tyrosine hydroxylase-immunopositive dopaminergic neurons. Our results provided evidence that **3b** might be a promising candidate for Parkinson's disease treatment.

1. Introduction

Parkinson's disease (PD) is one of the most common incurable neurodegenerative diseases, which affects about 1% of global elderly over sixty ages and more than 3% over eighty ages, that brings severe financial and society burden [1]. It has been characterized by cardinal motor symptoms, such as resting tremor, muscular rigidity, akinesia, and postural instability resulting from the loss of dopamine (DA) neurons in the substantia nigra (SN) and the depletion of the neurotransmitter DA in the striatum [2]. Currently, dopamine precursor levodopa [3] (dopaminergic agents) as well as adamantamine hydrochloride and cabergoline (direct or indirect dopamine agonist) are the most widely used drugs for PD treatment. Among the agents, levodopa remains the cornerstone for managing PD patients, especially in the early stages [4]. Other drugs are generally used in combination with levodopa to control specific symptoms or to enhance levodopa activity [3]. However, those drugs only ameliorate motor symptoms for a short period of time and even cause side effects, such as L-DOPA-induced dyskinesia, when taken for long periods [5,6]. So far, no drugs have been developed to slow or reverse the neurodegenerative process in PD [7]. Therefore, it is important to develop new therapies preventing the death of DA neurons in PD-affected brain areas.

Recently, the role of oxidative stress in neurological abnormalities, including PD, has been particularly addressed. Oxidative stress is a disturb of the balance of cellular antioxidant defense systems by over expression of reactive oxygen species (ROS) [8]. Nuclear factor erythroid 2-related factor 2 (Nrf2) is the master regulator of cellular defense against oxidative stress [9]. Under normal conditions, Nrf2 is rapidly degraded (half-life ~ 20min) by the Kelch like ECH-associated protein 1 (Keap1), an adaptor in the Cul3 (cullin3)-based ubiquitin E3 ligase, mediated ubiquitin proteasome system. Under stress conditions, oxidants and electrophiles react with

* Corresponding author.
** Corresponding author.
E-mail addresses: yhy1984_hb@163.com (H. Ye), chenlijuan125@163.com (L. Chen).
[1] These authors contributed equally.

https://doi.org/10.1016/j.ejmech.2020.112385
0223-5234/

cysteine sensors within Keap1, causing a conformational change of Keap1 and a detachment of Nrf2 from Keap1, which allows Nrf2 to translocate to the nucleus where Nrf2 binds to antioxidant responsive elements (ARE) via hetero-dimerization with small Maf proteins, activating the expression of its target genes, including several antioxidant and detoxification genes, such as heme oxygenase-1 (HO-1), superoxide dismutase (SOD), NAD(P)H: quinoneoxidoreductase (NQO1), the glutamate-cysteine ligasemodifer (GCLM) and the catalytic (GCLC) subunit [10,11]. Therefore, activating the Keap1/Nrf2 signaling pathway has been considered to be able to reduce and prevent neuronal cell death, representing a promising avenue for PD therapy [12,13].

Covalently modifying the thiol-rich Keap1 protein *via* electrophilic molecules is the major strategy for Nrf2 activation, which sparked the interest of the pharmaceutical industry and led to a substantial improvement in the clinical development of NRF2 modulators [9]. The first Nrf2-inducer dimethyl fumarate (Tecfidera) with the mechanism of reacting with Cys151 of Keap 1 protein has been approved by FDA for the treatment of remitting-relapsing multiple sclerosis and psoriasis [14,15]. CDDO, the first phase II clinical drug for the treatment of diabetic nephropathy, and its methyl ester (bardoxolone methyl or CDDO-Me), phase III for the treatment of chronic kidney disease and hypertension, pulmonary arterial are also thought to react with Cys151 for the activation of Nrf2 through its α,β-unsaturated scaffold [16]. Some other Nrf2 activators based on different scaffolds are under clinical development at various stages, such as cyanoenone triterpenoids, fumaric acid analogues, curcumin, and isothiocyanate sulforaphane (SFN) [16]. Thus, chemicals with electrophilic scaffold, especially α,β-unsaturated ketone structure, have the potentials for the treatment of PD through Nrf2 activation. Piperine (PIP) as a major alkaloid, isolated from the fruits of *Piper longum* and *Piper nigrum* [17],

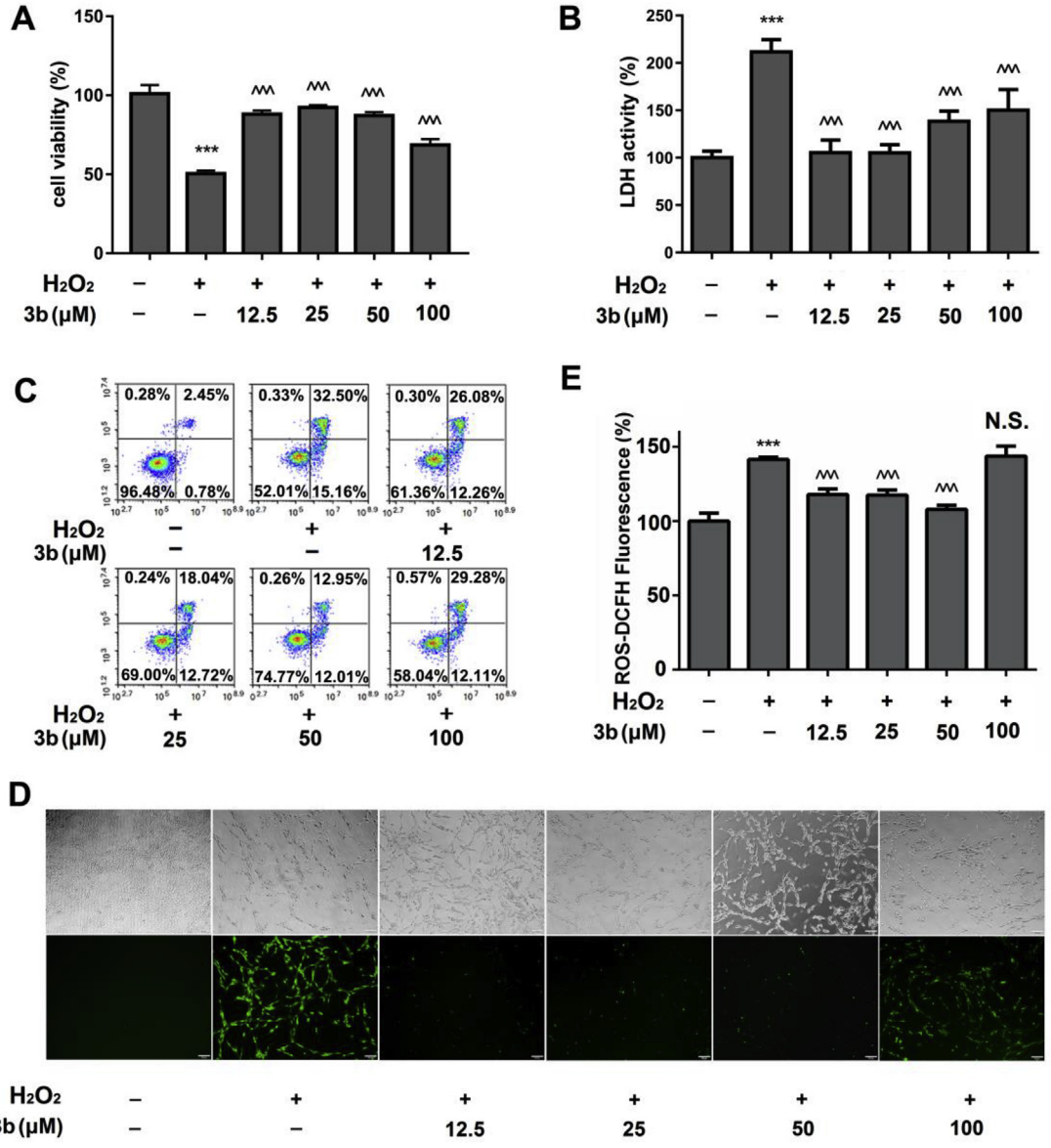

Fig. 1. Neuroprotective effect of **3b** against H_2O_2 induced PC12 cell damage. (A) The cytoprotection of **3b** in H_2O_2 induced PC12 cell damage, determined by MTT assays. (B) The effect on LDH release of **3b** in H_2O_2 induced PC12 cell damage. (C) The apoptosis inhibition effects of **3b**, determined by flow cytometry. (D, E) The ROS level in PC12 cells were assessed using DCFH-DA staining (D) and flow cytometry (E); The fluorescence images (bottom panel) indicated the elimination of H_2O_2-induced ROS in PC12 cells by **3b**. The corresponding phase contrast images were shown in the top panel. All data represent the means ± SD of three independent experiments. ***, $P < 0.001$ vs the vehicle group; ^^^, $P < 0.001$ vs the H_2O_2-treated group.

demonstrated various of biological activities [18–24]. Its α,β-unsaturated ketone structure makes a perfect lead for the Nrf2 activator development. Previously, PIP has been reported to exhibit good neuroprotective effects in both 1-methyl-4-phenyl-1,2,3,6-tetrahydropyridine hydrochloride (MPTP) or 6-OHDA induced Parkinson's animal models through antioxidant, anti-apoptotic and anti-inflammatory mechanism [25,26]. In order to improve the neuroprotective activity of PIP, we synthesized a series of PIP analogues following the strategy shown in Chart 2 and evaluated their neuroprotective activities in H_2O_2 induced PC12 cell damage model. Among the forty-one PIP derivatives, **3b** exhibited the best neuroprotective effect. The cellular assay showed that **3b** demonstrated cytoprotection effects *via* suppression of ROS accumulation and restoration of mitochondrial membrane potential in PC12 cells, which might be related to the activation of Nrf2 and the expression of corresponding antioxidant protein by promoting Nrf2 entry into the nucleus, thereby activating cellular oxidative stress and protecting PC12 cells. Moreover, the neuroprotective effect of **3b** was abolished when Nrf2 was knockdown by shRNA transfection, which further confirmed that Nrf2 was crucial for the neuroprotective effect of **3b**. Molecular docking study with the homology structure for the all length Keap1 constructed by I-TASSER online service also showed that **3b** might activate Nrf2 through covalently binding with Cys residues in Keap1 based on the lowest binding energy. In *in vivo* experiment, **3b** improved motor behavior and rescued dopaminergic neuronal cell death against MPTP induced PD mice model.

2. Results and discussion

2.1. Protection of PC12 cells against H_2O_2-induced cell damage by PIP analogues

Hydrogen peroxide (H_2O_2), an endogenous cellular signaling molecule could generate exogenous free radicals immediately [27]. Neuronal damage in the nervous system induced by abnormal high levels of H_2O_2 has been implicated in AD, PD and other neurodegenerative diseases [27]. Since H_2O_2 at concentration of 650 μM could induced approximate 50% PC12 cell damage (Fig. S1), it was then chosen for the further study. Neuroprotective effects of PIP analogues (12.5 μM) against H_2O_2-induced damage of PC12 cell were shown in Fig. 1 with TBHQ (*tert*-tutylhydroquinone) as the positive control.

As exhibited in Table 1, different substituted groups were introduced at the 2-, 3-, and 4-position of phenyl. In this series of analogues, the 2-methoxy substituted **3b** exhibited potency neuroprotective effect with cell viability (89%) better than **3c** and **3a** (2-OMe > 3-OMe > 4-OMe). However, when the methoxyl was substituted with hydroxyl group, compound **4c** substituted at the 3-position showed better neuroprotective effect than at 2-position, followed by 4-position substituted **4a** (3-OH > 2-OH > 4-OH). Along with these compounds, we also synthesize several compounds substituted with phenyl (**3f**), pyrrolidine (**3g**), piperazine (**3h**), morpholine (**3k**), piperidine (**3l**), and chlorine (**3m**). Unfortunately, only **3h** substituted with piperazine at 4-position of phenyl showed improved neuroprotective effect compared with piperine (**3n**) and most of the 4-substituted compounds showed only marginal or negative effect due to cytotoxicity (Table S1). To further explore the contribution of amide moiety to the neuroprotective effect, the piperidine of **3n**, **3b**, **3h** and **4a** was substituted with diethylamine or ethylamine. Unexpected, these compounds showed different structure-neuroprotection relationship. The neuroprotective effects of **3b**, **3h** and **3n** were abolished or decreased when the amide was substituted with diethylamine or ethylamine, while **4d** (67%) and **4e** (69%) showed improved activity compared with **4a**.

Heterocycles are common fragments of the vast majority of marketed drugs and play central roles in drug design [28–30]. The majority nature of heterocycles are served as hydrogen bond donors and receptors [28–30]. Thus, we further used heterocycles to replace the aromatic group in the scaffold of PIP, such as 2-furan (**3q**), 2-thiophene (**3r**) and *N*-methyl-2-pyrrole (**3u**). The results (Table 2) showed that **3s**, **3t** and **3v** exhibited improved activity with cell viability of 77%, 77% and 67% respectively, compared with PIP (**3n**) (56%) and when piperidine of **3r** was substituted with the diethylamine and ethylamine, the cell viability were obviously improved with 20%, which was in accordance with **4a**.

Since 2-Piperidinone (Chart 1), which contained shorter unsaturated chain compared with PIP, exhibited good neuroprotective activity [13]. We hypothesized that shorter unsaturated chain may be beneficial to improve the neuroprotective activity of PIP. To test the hypothesis, compound **7a**-**7n** were synthesized (Table 3). For the length of the unsaturated chain, there was no rules to follow at least within compounds that we reported. For instance, **7a** (73%), **7b** (69%), **7f** (77%), **7g** (72%) and **7h** (70%) with an unsaturated double bond has superior activity than corresponding two unsaturated double bonds compounds **3h** (65%), **3i** (64%), **3n** (56%), **3o** (31%) and **3p** (22%), while **7c** (43%), **7i** (81%), **7j** (78%), **7k** (68%), **7m** (54%) and 7**n** (57%) has lower activity than **3j** (61%), **3b** (89%), **3d** (81%), **3e** (75%), **3s** (77%) and **3t** (77%). In sum, the initial SARs study of PIP provided valuable information for further study of the neuroprotective effects of PIP analogues.

The property of blood-brain barrier (BBB) penetration is one of the primary challenges for neuroprotective agents *in vivo*. Hence, ADMET-BBB Level were calculated for all analogues to predict the BBB penetration ability based on the following parameters: (I) the calculated cLogP; (II) the calculated cLogD (at pH 7.4); (III) the most basic center (pKa); (IV) the molecular weight (MW), (VI) the topological polar surface area (TPSA) and the number of hydrogen bond donors (HBD) [31]. Results revealed that all the compounds showed high BBB penetration level (Tables S2 and S3). We also performed an *in vitro* BBB model using bEnd.3 cells to predict the membrane penetration of **3b** (Table S4). The permeability of **3b** (*Pe*: 3033.59×10^{-6} cm/s) was found to be better than that of piperine (*Pe*: 2551.95×10^{-6} cm/s). Considering **3b** demonstrated the best protection effects against H_2O_2-induced PC12 cell damage and good BBB permeability, its underlying mechanism was further evaluated.

2.2. Protection of PC12 cells from H_2O_2-induced damage by **3b**

The viability of PC12 cells treated by **3b** with the concentration ranging from 12.5 to 100 μM was first evaluated by MTT assay. Result showed that **3b** significantly elevated the cell viability from 72% to 91% at tested concentration compared with H_2O_2 treated group (51%) (Fig. 1A). Lactate dehydrogenase (LDH) was a critical marker for the membrane integrity. High content of LDH released in the medium implied cell damage [32]. In our experiment, H_2O_2 up-regulated the content of LDH almost two folds compared with the control. As we expected, **3b** decreased the release of LDH significantly in accordance with the cell viability (Fig. 1B). However, it could also be observed that higher concentration of **3b** (50 and 100 μM) demonstrated slight toxicity from the increasing LDH content.

2.3. Attenuation of apoptosis of PC12 cells induced by H_2O_2

To further evaluate whether apoptosis of PC12 cells induced by H_2O_2 could be attenuated by **3b**, cells were stained with Annexin V-FITC/PI and then analyzed by flow cytometry. As shown in Fig. 1C, compared with the H_2O_2 treated group (47.66%), percentage of apoptotic cells was significantly decreased in a dose-dependent

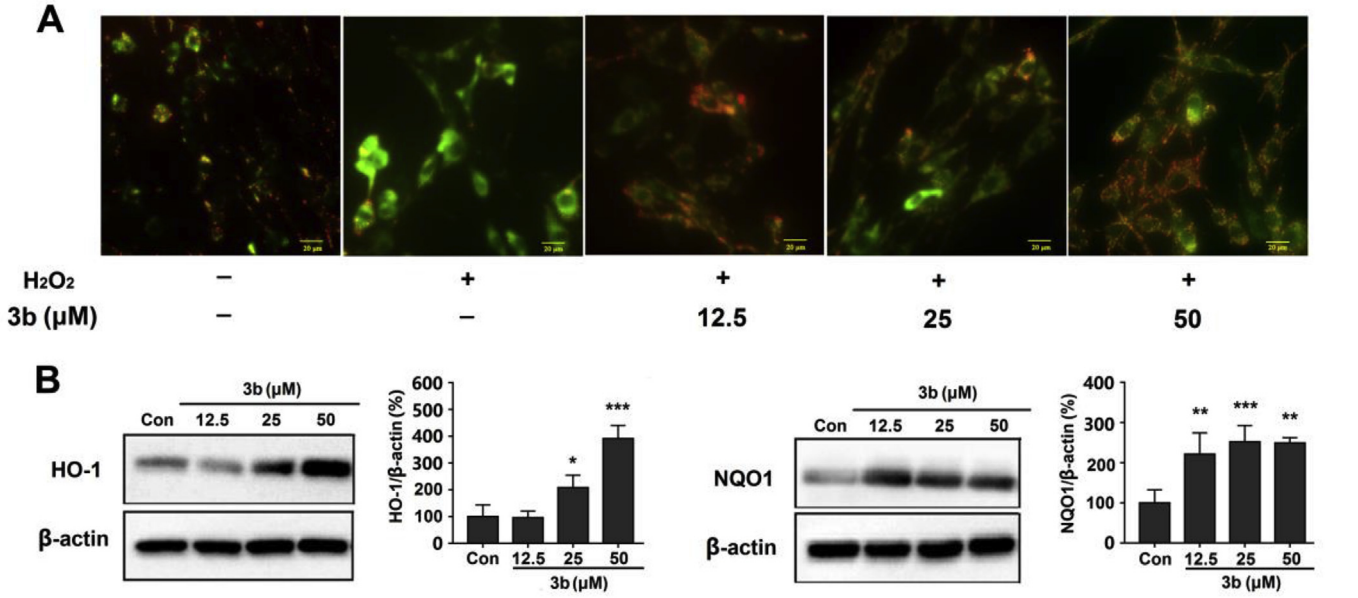

Fig. 2. **3b** could rescue the mitochondrial membrane potential in PC12 cells and upregulate the phase II antioxidant enzymes. (A) The mitochondrial membrane potential was measured by JC-1 stain. PC12 cells were pretreated with compound **3b** (12.5, 25 and 50 μM) for 24 h, induced with H_2O_2 for another 24 h and stained with JC-1. Data (red/green fluorescence ratios) were expressed as mean ± SD of three independent experiments. (B) **3b** induced the expression of NQO1 and HO-1. PC12 cells were treated with **3b** for 24 h, and the NQO1 and HO-1 were determined by Western blot. All data represent the means ± SD of three independent experiments. *, $P < 0.05$, **, $P < 0.01$, and ***, $P < 0.001$ vs the vehicle group; ^, $P < 0.05$ and ^^, $P < 0.01$ vs the H_2O_2-treated group. (For interpretation of the references to colour in this figure legend, the reader is referred to the Web version of this article.)

manner in groups pretreated by **3b** (12.5−50 μM). And in accordance with the results of LDH assay, percentage of apoptotic cells increased again at 100 μM due to cytoxicity. Taken together, **3b** could protect PC12 cell apoptosis induced by H_2O_2, but exhibited cytotoxicity at high concentration.

2.4. Prevention of ROS accumulation in PC12 cells

The imbalanced redox states caused by excessive reactive oxygen species (ROS) production is most widely implicated in PD [33]. Further experiments were performed to ascertain whether protection effects caused by **3b** were due to interference with ROS generation and reduction of the oxidative stress. Intracellular ROS accumulation can be measured by cell-permeable and nonfluorescent DCFH-DA. Once diffusing into cells, it is hydrolyzed by the cellular esterase activity to DCFH, which then interacts with ROS forming fluorescent 2′,7′-dichlorofluorescin [34]. Stimulation of PC12 cells with H_2O_2 led to appearance of bright-green fluorescence, indicating the burst of ROS in the cells compared with control group (Fig. 1D and E). Both the results of fluorescence and flow cytometry indicated that cells pretreated with **3b** (12.5, 25 and 50 μM) significantly reduced the accumulation of ROS induced by H_2O_2, while the accumulation of ROS was not reduced properly when pretreated with 100 μM **3b**. Consistent with the LDH assay and flow cytometry results, **3b** showed toxicity to cells at 100 μM. The result revealed that **3b** prevent the accumulation of ROS in PC12 cells. Further, 2,2-diphenyl-1-picrylhydrazyl (DPPH) assay was performed to determine the direct free radical scavenging activity of **3b** (Fig. S2). Results indicated that **3b** did not act as a direct free radical scavenger. The above results showed that the cytoprotection effects of **3b** might result from suppression of ROS accumulation in PC12 cells, but did not directly scavenge free radical.

2.5. Protective effect on H_2O_2-induced dissipation of the mitochondrial membrane potential

It is generally accepted that the mitochondrial membrane plays an important role in cell survival and death, especially under the influence of oxidative stress [9]. In this study, the membrane-permeant and sensitive JC-1 dye was used to monitor mitochondrial membrane potential ($\triangle\psi m$) of H_2O_2-induced PC12 cells (Fig. 2A), which formed red fluorescent J-aggregates in healthy cells with a normal $\triangle\psi m$ and retained its original green fluorescence under apoptotic condition. Our results suggested that mitochondrial membrane potential loss induced by H_2O_2 could be suppressed in a dose dependent manner by pretreatment with **3b**, indicating that the neuroprotection of **3b** might be related to the $\triangle\psi m$ restoration.

2.6. Activation of phase II antioxidant enzymes in PC12 cells

Phase II antioxidant enzymes provide efficient cytoprotection by regulating the intracellular redox state, including Heme oxygenase-1 (HO-1) and quinone oxidoreductase 1 (NQO1) and other enzymes [35]. NQO1 detoxifies benzene-derived quinones and generate antioxidant forms of ubiquinone and Vitamin E [32], while HO-1 catalyzes the initial and rate-limiting step in the degradation of heme into carbon monoxide, biliverdin/bilirubin, and ferritin [36]. Therefore, we hypothesized that ROS scavenging activity of **3b** attributed to induction of phase II enzymes. As showed in Fig. 2B, the HO-1 level pretreated by **3b** was remarkably upregulated compared with control group in a concentration-dependent manner, and the NQO1 level was also significantly upregulated, confirming our hypothesis that **3b** upregulated the antioxidative defense system to scavenge ROS.

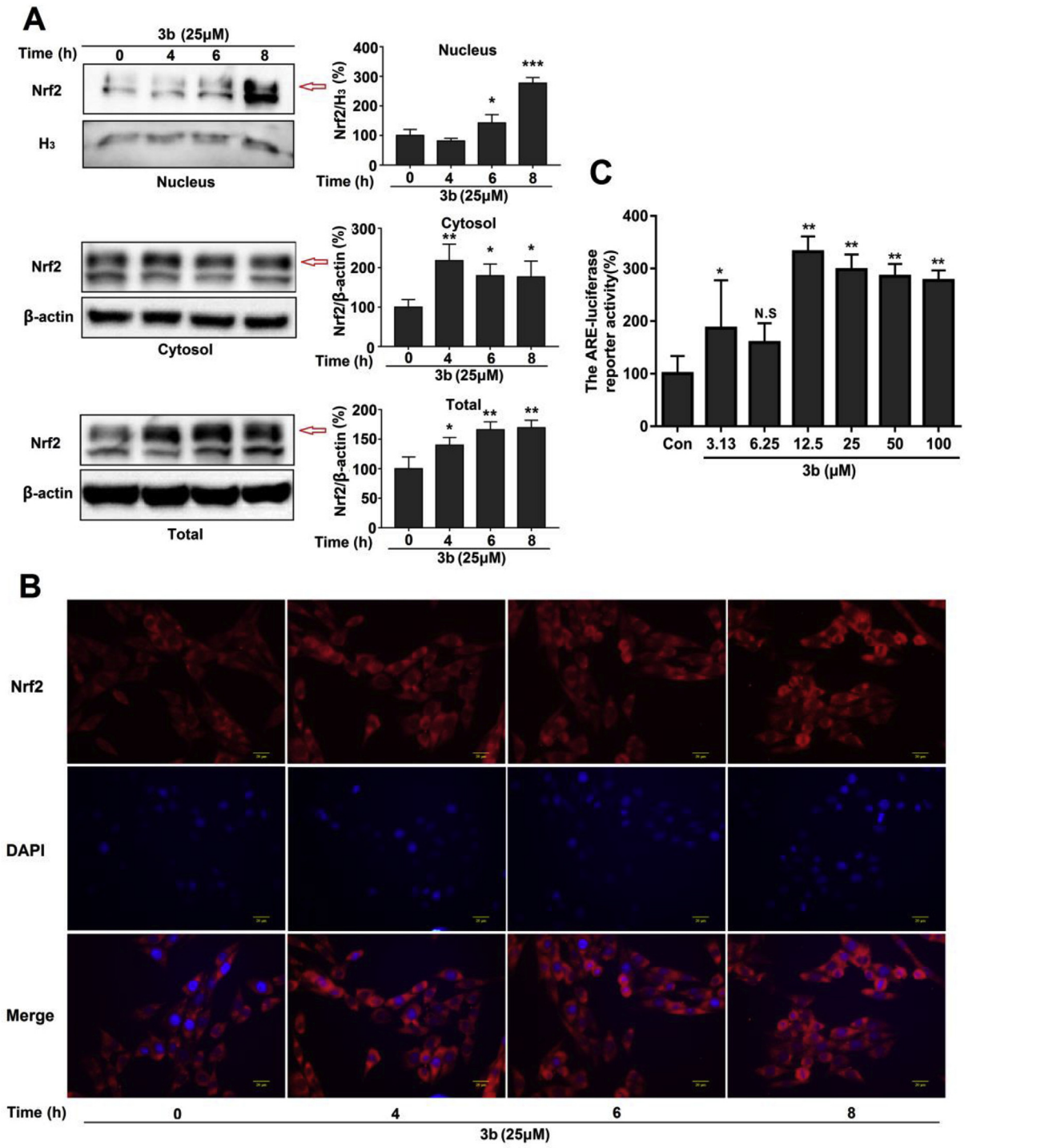

Fig. 3. The accumulation of Nrf2 in nucleus. (A) **3b** promoted Nrf2 translocation into the nucleus detected by Western blot assay. PC12 cells were incubated with **3b** at 25 μM for 4, 6 and 8 h. Nuclear Nrf2, cytosolic Nrf2, and total Nrf2 were prepared and analyzed by the western blots. (B) Nrf2 accumulation in the nucleus detected by immunofluorescence assays. PC12 cells were incubated with **3b** at 25 μM for 4, 6 and 8 h, and then stained with Nrf2 antibody and DAPI. (C) The inductivity of **3b** is calculated compared to the blank control. All data represent the means ± SD of three independent experiments. *, $P < 0.05$, **, $P < 0.01$, and ***, $P < 0.001$ vs the vehicle group.

2.7. Promotion of Nrf2 nuclear accumulation

Previous studies have determined that Nrf2 binds to a common DNA sequence called antioxidant response element (ARE) in nucleus to initiate the transcription of numerous cytoprotective proteins, including phase I and phase II drug-metabolizing enzymes, drug transporters, and antioxidants [11]. Hence, we examined whether **3b** could induce the nucleus translocation of Nrf2 in PC12 cells by Western blot assay (Fig. 3A). Results showed that treatment of PC12 cells with **3b** (25 μM) significantly promoted Nrf2 protein accumulation in the nucleus in a time dependent manner, which was in accordance with the immunofluorescence assays results (Fig. 3B), indicating that the protection effect of **3b** in PC12 cells might be due to promotion of Nrf2 accumulation in the

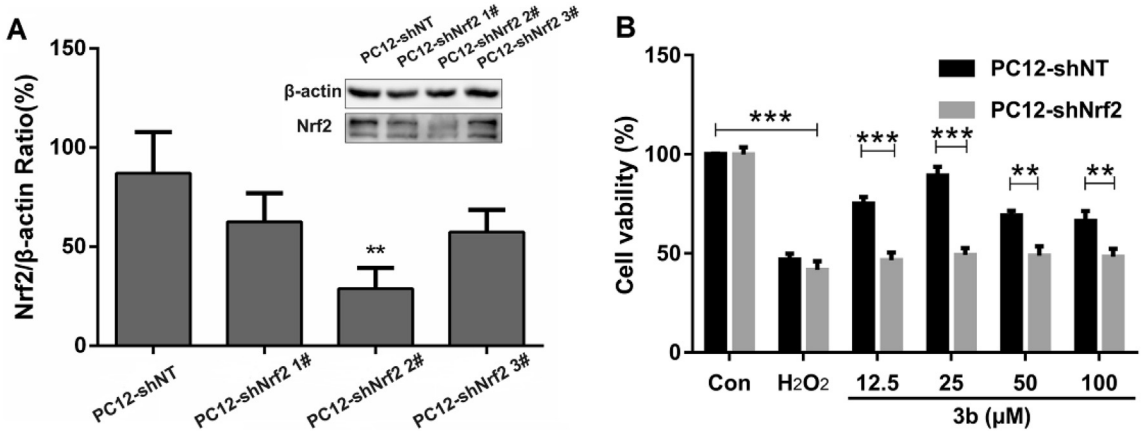

Fig. 4. Prerequisite of Nrf2 for the cytoprotection of **3b** in PC12 cells. (A) Expression level of Nrf2 in PC12-shNrf2-1, 2, 3 cells and PC12-shNT cells were determined by Western blot. (B) The cytoprotection of **3b** in H_2O_2 induced PC12-shNT cells and PC12-shNrf2-2 cells damage. Cells were pretreated with **3b** (12.5, 25.0, 50.0 and 100 μM) for 24 h and induced with H_2O_2 for another 24 h, then determined by MTT assays. All data represent the means ± SD of three independent experiments. **, $P < 0.01$, and ***, $P < 0.001$ vs the vehicle group.

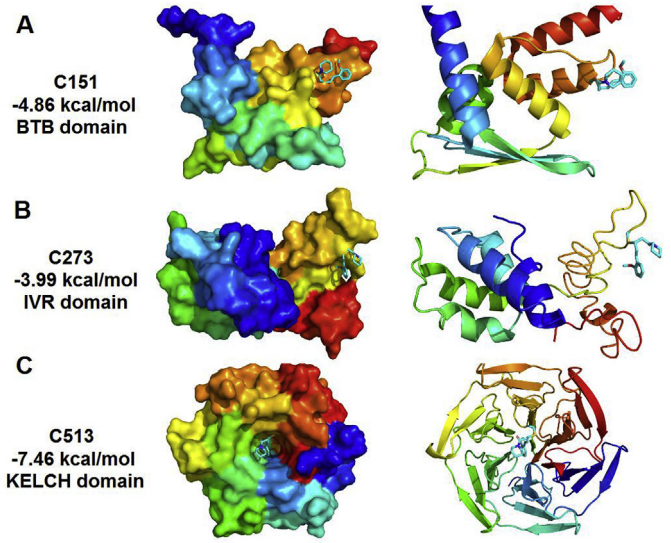

Fig. 5. In silico modeling of interaction of **3b** with representative Cys in Keap1. (A) Covalent docking of **3b** with Cys 151 in BTB domain (PDB 4CXT). (B) Covalent docking of **3b** with Cys 273 in IVR domain (PDB not available). (C) Covalent docking of **3b** with Cys 513 in Kelch domain (PDB 4IFL).

nucleus. HepG2 cell, transiently transfected with ARE-luciferase, were used for the evaluation of Nrf2-ARE activation effects of **3b**. **3b** exhibited ARE inductivity more than three-folds at 12.5 μM compared with control group, while no normal dose-dependent manner were observed, confirmed that **3b** effectively promotes Nrf2 nucleus translocation and ARE genes expression.

2.8. Prerequisite of Nrf2 for cytoprotection of *3b*

To further demonstrate the role of Nrf2 signaling pathway in the cellular protection effects of **3b** in PC12 cells, Nrf2 knockdown PC12 cells was constructed by infection of lentiviral carrying negative control shRNA (PC12-shNT) or Nrf2 shRNA (PC12-shNrf2-1, 2, 3). As seen in Fig. 4A, PC12-shNrf2-2 successfully silenced the expression level of Nrf2 detected by Western blot and then PC12-shNT and PC12-shNrf2-2 were chose for the further test. Silencing of Nrf2 expression was evaluated in Fig. 4B via Western blot assay. The protecting effect of **3b** was almost completely suppressed in the PC12-shNrf2-2 cells, while a clean promotion of cell viability in PC12-shNT cells pretreated by **3b** was observed, indicating that Nrf2 played an indispensable role in the cytoprotection of **3b** in PC12 cell.

2.9. Molecular docking study with Keap1

Nrf2 activation was tightly regulated by Keap 1 and many electrophiles chemicals were reported to modify the cysteine rich protein Keap1 and thereby mediate interactions with the Cul3/Rbx1 E3 ubiquitin ligase system and activation of Nrf2.[9] Considering **3b** contained a Michael receptor moiety, α,β-unsaturated ketone structure with the potential to assault cysteine residues in biomolecules, computational molecular docking methods were then used to predict the potential molecular interaction mechanisms between **3b** and Keap1 (Fig. 5 and Fig. S4 and Table S5). There are 27 Cys in Keap 1 included C77, C151 and C171 in the BTB domain and C368, C395, C406, C434, C489, C513, C518 and C583 in the Kelch domain (Fig. S3) with the other Cys residues located on the N-terminal, IVR domain and C-terminal [37]. Since no full length Keap 1 cristal structure was available, we selected the I-TASSER online service [38] to construct the homology structure for the full length Keap1. Upon applying covalent docking software (AutoDock 4.2) [39], which allowed to integrate Michael addition reactions of **3b** with all Cys residues in Keap1, lower binding energy was used as a criterion to predict the possible binding site between 3b and Keap 1. Consistent with the previous report that Cys151, Cys273, and Cys288 appeared to be the most susceptible cysteines to electrophile reaction [9], the binding energy for 3b with the three cysteines in our experiment were estimated with comparably low binding energy as −4.86, −3.99 and −3.97 kcal/mol, respectively. Except these common three cysteines, Cys513 and Cys368 were found as the potential binding site with the lowest binding energy (−7.46 kcal/mol and −6.86 kcal/mol) (Table S5). And the possible interaction mode of 3b with Cys151 in the BTB domain (4CXI), Cys249 and 288 in the IVR domain and Cys368, Cys513 in the Kelch domain (4IFL) were displayed in Fig. 5 and Fig. S4. Further confirmation experiment would be done in the near future. The above results suggesting that **3b** might have the potential to covalent binding with Keap1, alter the conformation of Keap1 leading to nuclear translocation of Nrf2 and subsequently activate the target gene expression. To confirm if **3b** can covalently bind with Keap1,

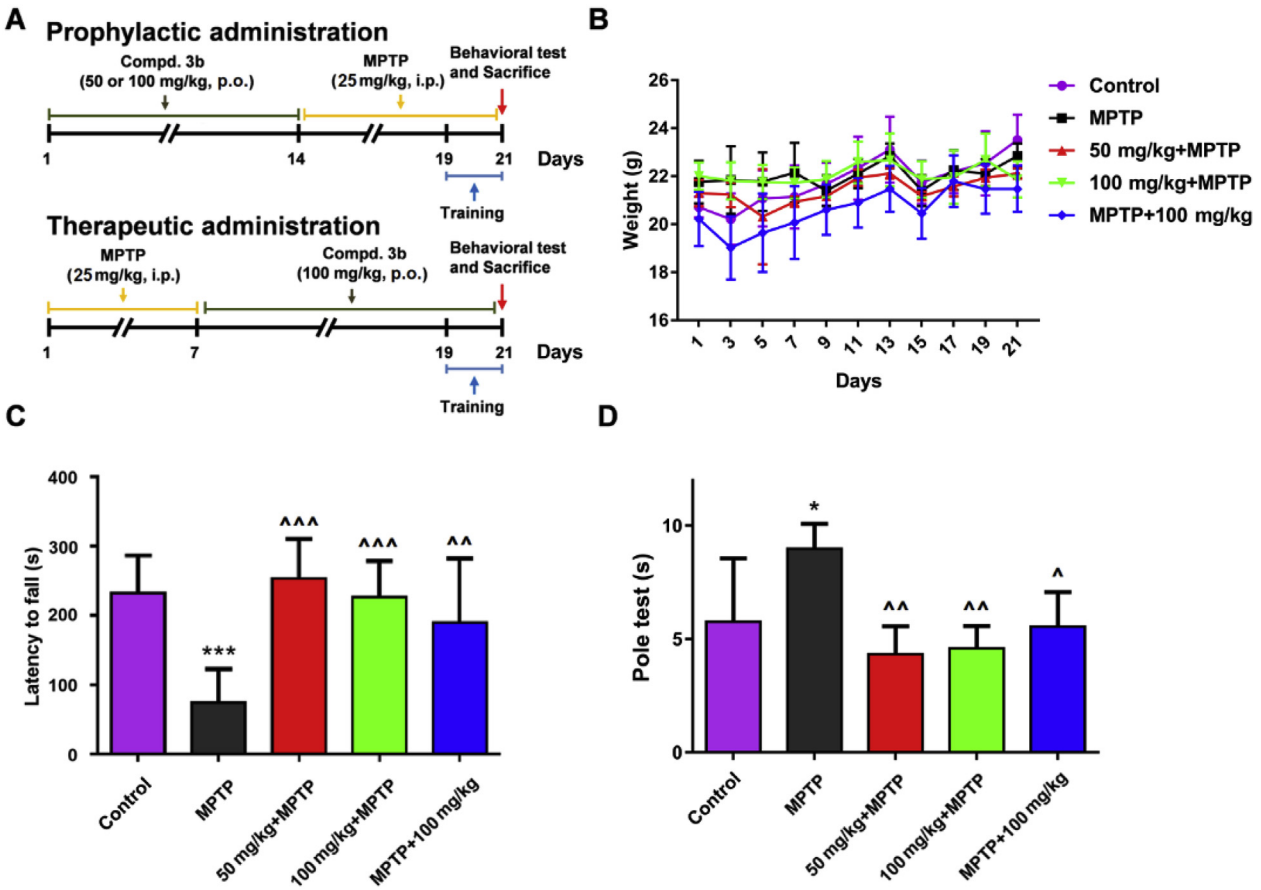

Fig. 6. **3b** attenuated the deficits of motor behaviors in MPTP-induced PD mice. (A) Experimental protocols for pole and rotarod behavioral tests. (B) The weight of mice during the experiment. (C) Latency to fall off the rotating rod in rotarod test. (D) Time that mice climb from the top to the bottom of the pole in pole test. All data represent the means ± SD of the mean (n = 6 per group). ***, $P < 0.001$ vs. the vehicle group; ^, $P < 0.05$, ^^, $P < 0.01$ and ^^^, $P < 0.001$ vs. the H_2O_2-treated group.

we performed LC-MS-MS analysis for **3b** incubated with recombinant full-length Keap1 (Fig. S5). Although the analysis showed **3b** can covalently bind with Cys288 within Keap1, it only have low confidence. Whether **3b** can covalently bind with Cys288 within Keap1 needs further experiment to confirm.

*2.10. **3b** improves motor behavior and rescues dopaminergic neuronal cell death in MPTP induced PD mice*

To determine **3b**'s effects on the behavioral recovery in MPTP-lesioned mice, motor behavior analysis was conducted through the rotarod and pole test. In the rotarod test (Fig. 6C), robust motor deficits were obviously observed in MPTP treated group, which was determined by decreased sustained rotarod time to 74.0 ± 48.2, a 68.9% decrease compared with the saline-treated control, whereas both prophylactic (50 and 100 mg/kg) and therapeutic administration (100 mg/kg) of **3b** significantly alleviated the abnormal movement with increased rotarod time to 253.7 ± 57.2, 226.2 ± 52.5 and 189.5 ± 92.7 s respectively. In the pole test (Fig. 6D), the MPTP treated group displayed a significant prolongation of the total time for climbing down the pole while prophylactic (50 and 100 mg/kg) and therapeutic administration (100 mg/kg) of **3b** reduced the climbing down time by 38.1%, 34.5% and 20.6% compared with MPTP treated group. Taken together, these behavioral results suggested that **3b** elicited a potent protective effect against MPTP-induced impairments in motor function while no obvious toxicity were observed (Fig. 6B).

Tyrosine hydroxylase (TH) is known to be involved in motor movement and is usually used as a marker for dopaminergic neurons [3]. Similar to the previous reports [25], the immunohistochemical staining for TH revealed that MPTP exerted significant neurotoxicity with 30.7% and 74.0% reduction of the TH-positive cells in the substantia nigra pars compacta (SNpc) and striatum respectively compared with the saline-treated control while both prophylactic (50 and 100 mg/kg) and therapeutic administration (100 mg/kg) of **3b** significantly increased the number of TH-positive cells (Fig. 7A), which was indicative of rescue on the MPTP-induced neurotoxicity, suggesting that **3b** might exhibit neuroprotective effects against dopaminergic neuronal cell death in PD. Since **3b** could active Nrf2 and its activation might protect neurons from dying in Parkinson's disease patients [40], the immunohistochemical staining for Nrf2 was also performed. It could be observed that Nrf2 was upregulated both in SNpc and striatum area in prophylactic (100 mg/kg) administration of **3b** (Fig. 7B). Nrf2 and its downstream protein, HO-1 and NQO1 in mouse brain tissue were further detected by western bolt. Fig. 8 showed that the expression of HO-1 and NQO1 was increased significantly by **3b**, indicating it could initiate the antioxidant system through Nrf2 activation *in vivo*, which was inconsistent with the *in vitro* results. The upregulation of antioxidative proteins HO-1 and NQO1 as well as the reverse of TH and Nrf2 in MPTP induced lesion in both striatum and SNpc area confirmed the neuroprotective and antioxidant effect of **3b**.

3. Conclusion

PIP as a natural alkaloid, isolated from the fruits of *Piper longum* and *Piper nigrum* [17], has been reported that it has the ability to

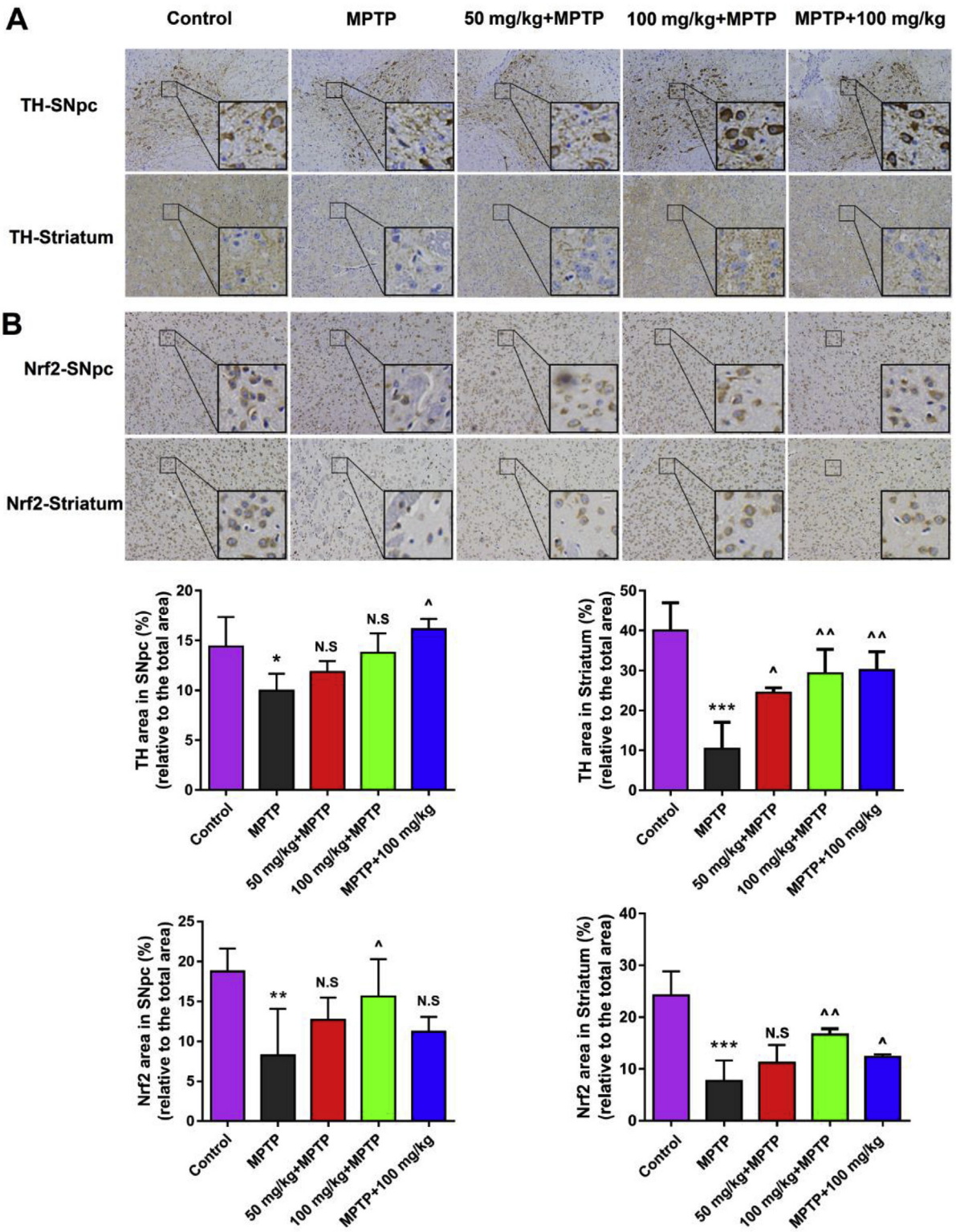

Fig. 7. 3b protected dopaminergic neurons and activated the antioxidant system in MPTP-induced PD mice. (A) Representative immunohistochemical staining (brown, TH) in the striatum and SNpc. Bar graphs summarized TH-immunopositive density to the total area. (B) Representative immunohistochemical staining (brown, Nrf2) in the striatum and SNpc. Bar graphs summarized Nrf2-immunopositive density to the total area. All data represent the means ± SD of the mean (n = 6). Magnification: × 100. *, $P < 0.05$, **, $P < 0.01$, and ***, $P < 0.001$ vs. the vehicle group; ^, $P < 0.05$ and ^^, $P < 0.01$ vs. the MPTP-treated group. (For interpretation of the references to colour in this figure legend, the reader is referred to the Web version of this article.)

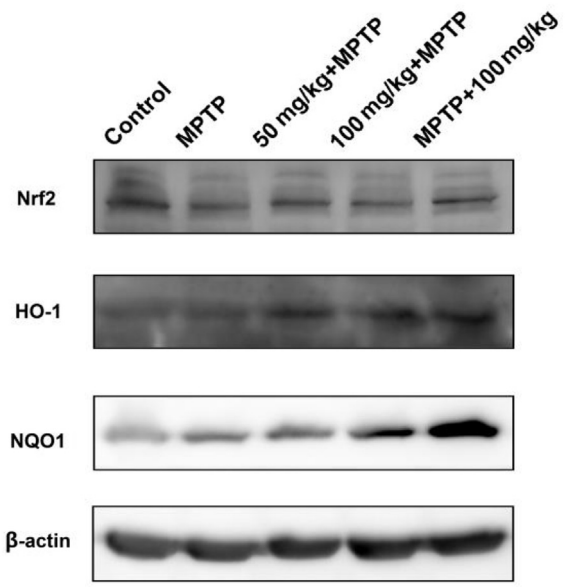

Fig. 8. **3b** induced the expression of Nrf2, NQO1 and HO-1 in MPTP-induced PD mice.

activate Nrf2 [41]ssss and has *in vivo* activity in MPTP or 6-OHDA induced PD mouse model [25,26]. However, the clinical usage was obstructed partially due to the low activity and undisclosed exacted mechanism [ref]. In order to improve the activity of PIP, a series of piperine analogues were designed and synthesized and their neuroprotective effects were evaluated in H_2O_2 induced PC12 cell damage model. The SAR investigation revealed that 2-methoxy substituted phenyl derivatives (**3b**) has the best activity and also indicated that further exploring the structure of aromatic group replaced with 2-thiophene and *N*-methyl-2-pyrrole maybe a promising strategy. **3b** with the best neuroprotective activity was chosen for the further mechanism research. Flow cytometry and fluorescence analysis showed that **3b** exhibited cytoprotection effects through suppression of ROS accumulation and restoration of mitochondrial membrane potential in PC12 cells. As DPPH assays showed that **3b** could not directly scavenge ROS, accompanied with upregulation of the phase II antioxidant enzymes HO-1 and NQO1 and previous report [41], we hypothesis that these effects may related to Nrf2-ARE signaling pathway. Western blot and immunofluorescence results showed that **3b** sinificantly promoted Nrf2 accumulation in the nucleus. Additionally, **3b** exhibited significant ARE inductivity in HepG2 cell, transiently transfected with ARE-luciferase.

Some reported Nrf2 activators can covalently modifying cysteine within Keap1 protein via Michael receptor, like the first Nrf2-inducer dimethyl fumarate (Tecfidera) can react with Cys151 of Keap1 protein to activate Nrf2, identified by LC-MS-MS analysis [15]. Considering **3b** also contains a Michael receptor moiety, α,β-unsaturated ketone structure with the potential to assault cysteine residues in biomolecules, computational molecular docking methods were applicated for identity the potential covalent binding target within Keap1 which tightly regulates Nrf2 activation.

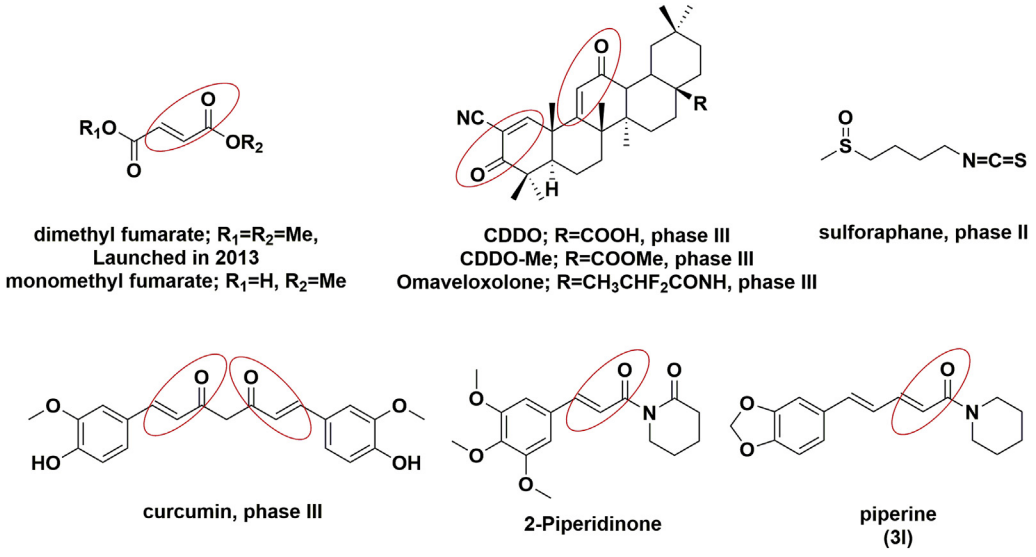

Chart 1. Known Keap1–Nrf2 pathway electrophilic activator bearing α,β-unsaturated ketone structure.

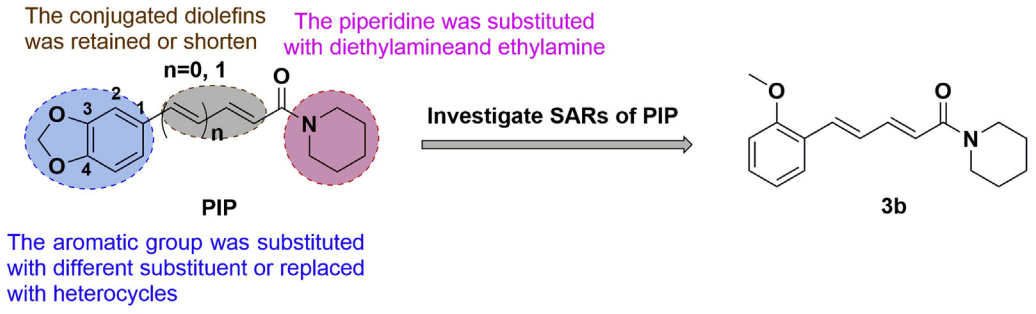

Chart 2. Strategy for structure optimization of PIP.

Table 1
The neuroprotection and ADMET-BBB level of PIP analogues substituted with different groups.

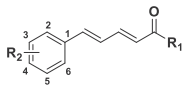

Compound	R_1	R_2	Cell viability (%) [a] (H_2O_2-induced PC12 cells)	ADMET-BBB Level [b]
H_2O_2			52.81 ± 6.00	
TBHQ			70.42 ± 2.01	
Piperine (**3n**)			55.72 ± 1.35	1
3a		4-OCH_3	26.47 ± 3.91	1
3b		2-OCH_3	88.82 ± 7.83	1
3c		3-OCH_3	58.12 ± 1.83	1
3d		2-OCH_3	80.74 ± 4.20	1
3e		2-OCH_3	74.62 ± 2.52	2
3f			15.15 ± 0.24	0
3g			37.20 ± 1.95	1
3h			64.99 ± 4.00	1
3i			63.56 ± 1.62	1
3j			60.79 ± 7.31	2
3k			20.18 ± 1.63	1
3l			18.86 ± 1.06	0
3m		4-Cl	32.14 ± 4.13	1
3o			31.41 ± 6.29	1
3p			22.31 ± 3.23	2
4a		4-OH	48.40 ± 1.63	1
4b		2-OH	68.84 ± 4.58	1
4c	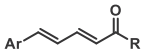	3-OH	75.67 ± 3.95	1
4d		4-OH	67.31 ± 2.20	1
4e		4-OH	69.14 ± 6.37	2

[a] Cell viability (%) were detected with compounds at the concentration of 12.5 μM; data are expressed as the mean ± SD of at least three independent experiments.
[b] the ADMET-BBB level was calculated by Discovery studio 3.1.

Table 2
The neuroprotection and ADMET-BBB level of PIP analogues substituted with heterocycles.

Compound	Ar	R	Cell viability (%) [a] (H_2O_2-induced PC12 cells)	ADMET-BBB Level [b]
H_2O_2			52.81 ± 6.00	
3q			33.29 ± 2.66	1
3r			57.88 ± 1.83	1
3s			77.33 ± 6.66	1
3t			77.22 ± 9.83	1
3u			40.95 ± 3.05	1
3v			67.83 ± 3.65	1
3w	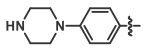		53.81 ± 4.04	1

[a] Cell viability (%) were detected with compounds at the concentration of 12.5 μM; data are expressed as the mean ± SD of at least three independent experiments.
[b] the ADMET-BBB level was calculated by Discovery studio 3.1.

Docking study with the homology structure for the all length Keap1 showed that **3b** might activates Nrf2 through covalently binding with Cys residues in Keap1 based on the lowest binding energy. However, our preliminary LC-MS-MS experiment showed that **3b** covalently binding to Keap1 is a low confidence result, although some peptides within Keap1 modified by **3b** can be detected. Future work is required to explore the condition of the LC-MS-MS experiment or adopt crystall structure or site-directed mutagenesis to further confirm the hypothesis. *In vivo*, **3b** improved motor behavior and rescued dopaminergic neuronal cell death in MPTP induced PD mice.

In a word, this work identified a promising candidate for the development of a novel therapeutic for PD, numbered as **3b**, which activated Nrf2-ARE signaling pathway may via covalently binding with Cys288 within Keap1.

4. Experiment part

4.1. Chemistry

All commercially available reagents were used without further purification. All solvents were dried and redistilled prior to use in the usual manner. Reaction progress was monitored using analytical thin layer chromatography (TLC) on precoated silica gel GF254 (Yantai, China) plates and the spots were detected under UV light (254 nm and 360 nm). Column chromatography was performed on silica gel (200–300 mesh, Yantai, China). ^{1}H and ^{13}C NMR spectra were on a Bruker Avance 400 spectrometer (Bruker Company, Germany), using TMS as an internal standard. Chemical shifts are reported in *ppm* (d) using the residual solvent line as internal standard. Splitting patterns are designed as s, singlet; d, doublet; t, triplet; m, multiplet. Mass spectra were recorded on a Q-TOF Premier mass spectrometer (Micromass, Manchester, UK). The purity of all compounds (>95%) was determined on a Waters e2695 series LC system (column, Agilent C_{18}, 4.6 mm × 150 mm, 5 μm; flow rate, 1.0 mL/min; UV wavelength, 254–400 nm; temperature, 25 °C; injection volume, 10 μL).

PIP analogues synthesized with the synthetic routes of the target compounds (**3a-w**, **4a-e**) depicted in Scheme 1. Briefly, commercially available (*E*)-2-crotonyl chloride was reacted with corresponding amines to form crotonyl amides **2a-c** [41], which was then coupled with substituted benzaldehyde (or aromatic heterocyclic formaldehyde) using NaOH to achieve the target molecules **3a-v** [41]. Target compounds **4a-e** need further reaction to demethylate in the presence of Boron tribromide (BBr_3) [42]. Synthesis of compound **7a-7n** is described in Scheme 2. The starting material, commercially available substituted benzaldehyde (or aromatic heterocyclic formaldehyde), reacting with malonic acid to obtain α,β-unsaturated acids **6a-e** through Knoevenagel reaction [13]. It was then coupled with corresponding amides to achieve the target molecules **7d-n** [13]. And some of the target molecules needed further reaction to deprotect with trifluoroacetic acid to obtain **7a-c**.

4.1.1. General procedure A for the synthesis of *2*

To a stirred solution of corresponding lamins (0.58 mol) and Et_3N (55 g, 0.4175 mol) in DCM (50 mL), crotonyl chloride (**1**) was added dropwise at 0 °C. After the addition, reaction mixture was slowly warm to room temperature and stirred for 8 h. Progress of the reaction was monitored by TLC. After completion, organic layer was washed with sat. sodium bicarbonate solution, water, dried over anhyd. Na_2SO_4 and concentrated under reduced pressure. A pale yellow viscous liquid **2** was obtained without further purified.

4.1.2. (E)-1-(piperidin-1-yl)but-2-en-1-one (*2a*)

Piperidine was reacted with crotonyl chloride (**1**) following the general procedure A to give the desired product **2a** as a light yellow oil (yield 98.0%). ^{1}H NMR (400 MHz, $CDCl_3$) δ 6.58 (dq, J = 13.9, 6.8 Hz, 1H), 6.06 (d, J = 15.0 Hz, 1H), 3.31 (d, J = 34.4 Hz, 4H), 1.64 (d, J = 6.8 Hz, 3H), 1.42 (dd, J = 10.7, 5.7 Hz, 2H), 1.33 (d, J = 4.8 Hz, 4H).

Table 3
The neuroprotection and ADMET-BBB level of PIP analogues.

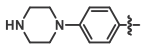

Compound	Ar	R	Cell viability (%) [a] (H_2O_2-induced PC12 cells)	ADMET-BBB Level [b]
7a		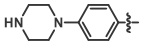	72.61 ± 3.37	2
7b		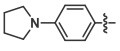	69.07 ± 2.03	2
7c		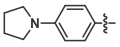	42.70 ± 1.77	2
7d			30.64 ± 0.51	1
7e			26.06 ± 1.98	1
7f			76.95 ± 4.73	2
7g			71.74 ± 7.15	2
7h			69.74 ± 8.74	2
7i			81.26 ± 2.61	1
7j			78.21 ± 2.13	1
7k			68.45 ± 1.56	2
7l			50.42 ± 3.18	1
7m			54.33 ± 1.90	1
7n			56.55 ± 4.79	2

[a] Cell viability (%) were detected with compounds at the concentration of 12.5 μM; data are expressed as the mean ± SD of at least three independent experiments.
[b] the ADMET-BBB level was caculated by Discovery studio 3.1.

Exact mass calcd for C9H15NO $[M+H]^+$: 154.1232; found 154.1235.

*4.1.3. (E)-N,N-diethylbut-2-enamide (**2b**)*

Diethylamine was reacted with crotonyl chloride (**1**) following the general procedure A to give the desired product **2b** as a light yellow oil (yield 98.0%). ^{1}H NMR (400 MHz, $CDCl_3$) δ 6.91–6.77 (m, 1H), 6.16 (dd, J = 14.9, 1.6 Hz, 1H), 3.41–3.27 (m, 4H), 1.81 (dd, J = 6.8, 1.6 Hz, 3H), 1.11 (dt, J = 20.7, 6.4 Hz, 6H). Exact mass calcd for C8H15NO $[M+H]^+$: 142.1232; found 142.1234.

*4.1.4. (E)-N-ethylbut-2-enamide (**2c**)*

Ethylamine was reacted with crotonyl chloride (**1**) following the general procedure A to give the desired product **2c** as a light yellow oil (yield 98.0%). ^{1}H NMR (400 MHz, $CDCl_3$) δ 6.80–6.62 (m, 1H), 5.79 (dd, J = 15.2, 1.6 Hz, 1H), 3.30–3.20 (m, 2H), 1.74 (d, J = 6.9 Hz, 3H), 1.06 (t, J = 7.3 Hz, 3H). Exact mass calcd for C6H11NO $[M+H]^+$: 114.0919; found 114.0918.

*4.1.5. General procedure B for the synthesis of **3***

To a stirred solution of aromatic aldehyde (1.0 equiv, 2.4 mmol) in DMSO (2 mL), 1 mL saturate sodium hydroxide solution was added and stirred for 30 min. Then **2** (1.0 equiv, 2.4 mmol) was added. Then stirred for another 6–8 h at room temperature. Reaction was monitored by TLC. After completion, the reaction mixture was quenched with 5% aq. HCl and extracted with DCM, washed with water, dried over anhyd. Na_2SO_4 and concentrated under reduced pressure. The obtained crude product was purified by column chromatography.

*4.1.6. (2E,4E)-5-(4-methoxyphenyl)-1-(piperidin-1-yl)penta-2,4-dien-1-one (**3a**)*

2a was reacted with 4-methoxybenzaldehyde following the general procedure B to give the desired product **3a** as a white powder (yield 88.0%). ^{1}H NMR (400 MHz, $CDCl_3$) δ 7.43 (ddd, J = 12.4, 6.3, 1.7 Hz, 1H), 7.40–7.37 (m, 2H), 6.89–6.85 (m, 2H), 6.81–6.77 (m, 2H), 6.43 (d, J = 14.6 Hz, 1H), 3.81 (s, 3H), 3.58 (s, 4H), 1.70–1.63 (m, 2H), 1.58 (dt, J = 11.0, 5.5 Hz, 4H). ^{13}C NMR (101 MHz,

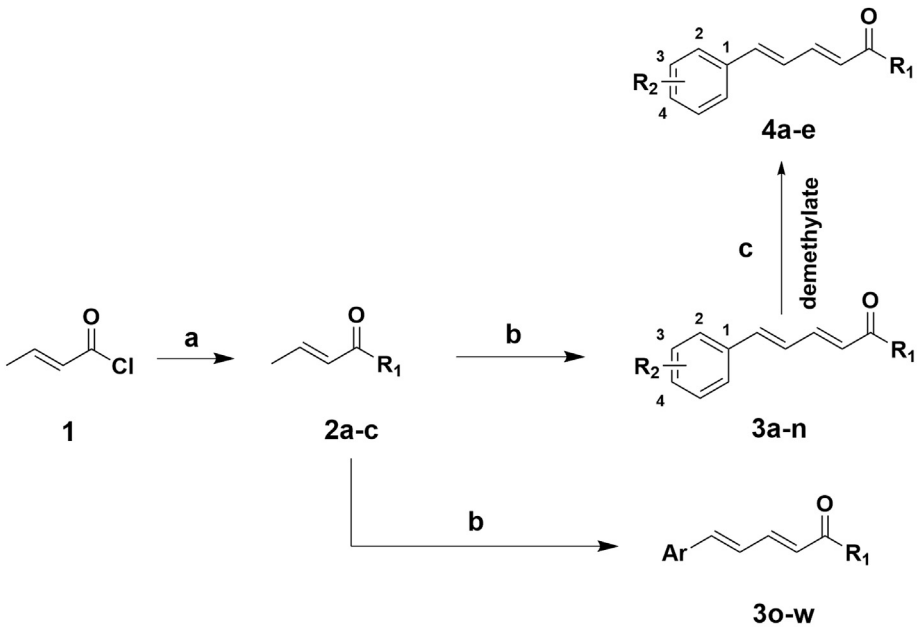

Scheme 1. Reagents and conditions: (a) Amines, Et_3N, CH_2Cl_2, 0 °C, 8 h; (b) Aromatic aldehydes, sat. NaOH, DMSO, r.t., 6–8 h; (c) 1M BBr_3, dry CH_2Cl_2, -80 °C, 6 h.

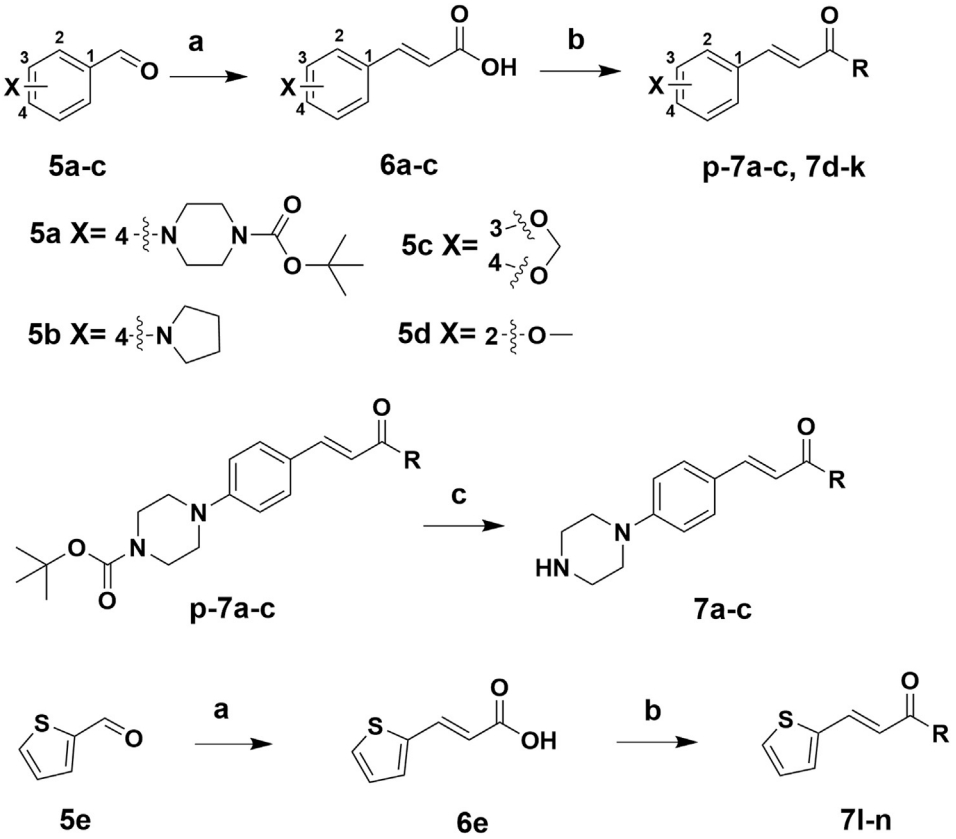

Scheme 2. Reagents and conditions: (a) Malonic acid, Piperidine, Pyridine, reflux, 8 h; (b) Amines, HATU, DMF, r.t., 4 h; (c) TFA, r.t., 2 h.

$CDCl_3$) δ 165.61, 160.12, 142.87, 138.30, 129.38, 128.40, 125.07, 119.72, 114.29, 55.40, 47.04, 43.54, 26.21, 24.76. Exact mass calcd for C17H21NO2 $[M+H]^+$: 272.1572; found 272.1576.

*4.1.7. (2E,4E)-5-(2-methoxyphenyl)-1-(piperidin-1-yl)penta-2,4-dien-1-one (**3b**)*

2a was reacted with 2-methoxybenzaldehyde following the general procedure B to give the desired product **3b** as a white

powder (yield 78.0%). ^{1}H NMR (400 MHz, $CDCl_3$) δ 7.42 (dd, J = 14.5, 10.3 Hz, 1H), 7.28–7.22 (m, 1H), 7.04 (d, J = 7.7 Hz, 1H), 6.97 (s, 1H), 6.94–6.77 (m, 3H), 6.49 (d, J = 14.7 Hz, 1H), 3.82 (s, 3H), 3.59 (s, 4H), 1.74–1.64 (m, 2H), 1.63–1.51 (m, 4H). ^{13}C NMR (101 MHz, $CDCl_3$) δ 165.48, 159.97, 142.33, 138.48, 137.99, 129.80, 127.48, 121.25, 119.77, 114.47, 112.13, 55.38, 47.05, 43.39, 26.80, 25.88, 24.76. Exact mass calcd for C17H21NO2 $[M+H]^+$: 272.1572; found 272.1576.

4.1.8. (2E,4E)-5-(3-methoxyphenyl)-1-(piperidin-1-yl)penta-2,4-dien-1-one (**3c**)

2a was reacted with 3-methoxybenzaldehyde following the general procedure B to give the desired product **3c** as a white powder (yield 76.0%). ^{1}H NMR (400 MHz, $CDCl_3$) δ 7.48 (dd, J = 7.6, 1.6 Hz, 1H), 7.45 (dd, J = 14.8, 11.2 Hz, 1H), 7.28–7.23 (m, 1H), 7.18 (d, J = 15.7 Hz, 1H), 7.00–6.91 (m, 2H), 6.88 (d, J = 8.3 Hz, 1H), 6.45 (d, J = 14.8 Hz, 1H), 3.87 (s, 3H), 3.58 (m, 4H), 1.71–1.63 (m, 2H), 1.59 (dt, J = 10.9, 5.4 Hz, 4H). ^{13}C NMR (101 MHz, $CDCl_3$) δ 165.67, 157.45, 143.37, 133.82, 129.74, 127.81, 127.32, 125.61, 120.79, 120.37, 111.18, 55.61, 47.04, 43.35, 26.84, 25.74, 24.79. Exact mass calcd for C17H21NO2 $[M+H]^+$: 272.1572; found 272.1576.

4.1.9. (2E,4E)-N,N-diethyl-5-(2-methoxyphenyl)penta-2,4-dienamide (**3d**)

2b was reacted with 2-methoxybenzaldehyde following the general procedure B to give the desired product **3d** as a white powder (yield 78.9%). ^{1}H NMR (400 MHz, $CDCl_3$) δ 7.57–7.44 (m, 2H), 7.30–7.15 (m, 2H), 7.03–6.90 (m, 2H), 6.88 (d, J = 8.3 Hz, 1H), 6.37 (d, J = 14.6 Hz, 1H), 3.86 (s, 3H), 3.53–3.36 (m, 4H), 1.24–1.13 (m, 6H). ^{13}C NMR (101 MHz, $CDCl_3$) δ 166.05, 157.39, 143.40, 134.03, 129.73, 127.67, 127.26, 125.50, 120.71, 120.40, 111.13, 55.55, 42.27, 41.00, 15.03, 13.29. Exact mass calcd for C16H21NO2 $[M+H]^+$: 260.1651; found 260.1649.

4.1.10. (2E,4E)-N-ethyl-5-(2-methoxyphenyl)penta-2,4-dienamide (**3e**)

2c was reacted with 2-methoxybenzaldehyde following the general procedure B to give the desired product **3e** as a white powder (yield 78.9%). ^{1}H NMR (400 MHz, DMSO-d_6) δ 8.01 (t, J = 5.4 Hz, 1H), 7.60 (dd, J = 7.7, 1.4 Hz, 1H), 7.34–7.25 (m, 1H), 7.17 (dd, J = 14.9, 10.7 Hz, 1H), 7.11 (d, J = 15.6 Hz, 1H), 7.04 (d, J = 2.2 Hz, 1H), 7.02–6.97 (m, 1H), 6.95 (t, J = 7.5 Hz, 1H), 6.09 (d, J = 14.9 Hz, 1H), 3.83 (s, 3H), 3.21–3.10 (m, 2H), 1.05 (t, J = 7.2 Hz, 3H). ^{13}C NMR (101 MHz, DMSO-d_6) δ 164.89, 156.77, 139.42, 132.44, 129.85, 127.43, 126.98, 125.23, 124.64, 120.61, 111.52, 55.52, 33.44, 14.75. Exact mass calcd for C14H17NO2 $[M+H]^+$: 232.1338; found 232.1338.

4.1.11. (2E,4E)-5-([1,1′-biphenyl]-4-yl)-1-(piperidin-1-yl)penta-2,4-dien-1-one (**3f**)

2a was reacted with [1,1′-biphenyl]-4-carbaldehyde following the general procedure B to give the desired product **3f** as a white powder (yield 68.5%). ^{1}H NMR (400 MHz, $CDCl_3$) δ 7.63–7.56 (m, 4H), 7.52 (d, J = 8.4 Hz, 2H), 7.49–7.40 (m, 3H), 7.36 (dt, J = 9.3, 4.2 Hz, 1H), 6.95 (dd, J = 15.5, 10.1 Hz, 1H), 6.88 (d, J = 15.5 Hz, 1H), 6.50 (d, J = 14.7 Hz, 1H), 3.60 (d, J = 40.1 Hz, 4H), 1.73–1.64 (m, 2H), 1.60 (m, 4H). ^{13}C NMR (101 MHz, $CDCl_3$) δ 165.37, 142.35, 141.28, 140.46, 138.02, 135.53, 128.85, 127.54, 127.41, 127.09, 126.95, 120.94, 46.98, 43.29, 26.77, 25.64, 24.69. Exact mass calcd for C22H23NO $[M+Na]^+$: 340.1677; found 340.1685.

4.1.12. (2E,4E)-1-(piperidin-1-yl)-5-(4-(pyrrolidin-1-yl)phenyl)penta-2,4-dien-1-one (**3g**)

2a was reacted with 4-(pyrrolidin-1-yl)benzaldehyde following the general procedure B to give the desired product **3g** as a white powder (yield 63.2%). ^{1}H NMR (400 MHz, $CDCl_3$) δ 7.44 (dd, J = 14.6, 10.5 Hz, 1H), 7.33 (d, J = 8.7 Hz, 2H), 6.78 (d, J = 15.4 Hz, 1H), 6.70 (dd, J = 15.4, 10.5 Hz, 1H), 6.52 (d, J = 8.6 Hz, 2H), 6.35 (d, J = 14.6 Hz, 1H), 3.58 (m, 4H), 3.35–3.28 (m, 4H), 2.03–1.98 (m, 4H), 1.69–1.63 (m, 2H), 1.61–1.53 (m, 4H). ^{13}C NMR (101 MHz, $CDCl_3$) δ 166.01, 148.23, 143.81, 139.70, 128.56, 122.16, 117.61, 111.88, 47.74, 46.96, 43.30, 26.82, 25.56, 24.85. Exact mass calcd for C20H26N2O $[M+Na]^+$: 333.1947; found 333.1947.

4.1.13. (2E,4E)-5-(4-(piperazin-1-yl)phenyl)-1-(piperidin-1-yl)penta-2,4-dien-1-one (**3h**)

2a was reacted with *tert*-butyl 4-(4-formylphenyl)piperazine-1-carboxylate following the general procedure B to give the intermediate **p-3h**. Then the intermediate **p-3h** was dissolved in 2 mL trifluoroacetic acid (TFA) and stirred for 1 h. After the reaction was completed, the reaction was quenched by saturated sodium bicarbonate solution and extracted with ethyl acetate (10 mL × 3), dried over anhyd. Na_2SO_4 and concentrated under reduced pressure to obtain the desired product **3h** as a light yellow powder (yield 68.5% over two steps). ^{1}H NMR (400 MHz, $CDCl_3$) δ 7.37 (dd, J = 9.3, 4.5 Hz, 1H), 7.33 (d, J = 8.6 Hz, 2H), 6.82 (d, J = 8.6 Hz, 2H), 6.77–6.73 (m, 2H), 6.39 (d, J = 14.7 Hz, 1H), 3.57 (s, 4H), 3.40 (s, 4H), 3.30 (s, 4H), 1.64 (m, 2H), 1.58 (m, 4H). ^{13}C NMR (101 MHz, $CDCl_3$) δ 166.39, 150.08, 143.77, 138.98, 129.46, 128.51, 125.01, 119.13, 116.71, 46.23, 45.27, 43.88, 43.44, 26.47, 25.87, 24.56. Exact mass calcd for C20H26N2O $[M+Na]^+$: 348.2052; found 348.2056.

4.1.14. (2E,4E)-N,N-diethyl-5-(4-(piperazin-1-yl)phenyl)penta-2,4-dienamide (**3i**)

2b was reacted with *tert*-butyl 4-(4-formylphenyl)piperazine-1-carboxylate following the general procedure B to give the intermediate **p-3i**. Then the intermediate **p-3i** was dissolved in 2 mL trifluoroacetic acid (TFA) and stirred for 1 h. After the reaction was completed, the reaction was quenched by saturated sodium bicarbonate solution and extracted with ethyl acetate (10 mL × 3), dried over anhyd. Na_2SO_4 and concentrated under reduced pressure to obtain the desired product **3i** as a light yellow powder (yield 68.5% over two steps). ^{1}H NMR (400 MHz, $CDCl_3$) δ 7.46 (ddd, J = 14.6, 6.1, 3.8 Hz, 1H), 7.38 (d, J = 8.6 Hz, 2H), 6.87 (d, J = 8.6 Hz, 2H), 6.83–6.75 (m, 2H), 6.34 (d, J = 14.6 Hz, 1H), 3.43 (m, 8H), 3.23 (d, J = 4.7 Hz, 4H), 1.21 (m, 6H), 0.91–0.79 (m, 1H). ^{13}C NMR (101 MHz, $CDCl_3$) δ 166.17, 147.66, 143.01, 138.55, 130.53, 128.36, 125.00, 119.83, 116.45, 47.73, 44.41, 42.38, 41.15. Exact mass calcd for C19H27N3O $[M+Na]^+$: 336.2052; found 336.2005.

4.1.15. (2E,4E)-N-ethyl-5-(4-(piperazin-1-yl)phenyl)penta-2,4-dienamide (**3j**)

2d was reacted with *tert*-butyl 4-(4-formylphenyl)piperazine-1-carboxylate following the general procedure B to give the intermediate **p-3j**. Then the intermediate **p-3j** was dissolved in 2 mL trifluoroacetic acid (TFA) and stirred for 1 h. After the reaction was completed, the reaction was quenched by saturated sodium bicarbonate solution and extracted with ethyl acetate (10 mL × 3), dried over anhyd. Na_2SO_4 and concentrated under reduced pressure to obtain the desired product **3j** as a light yellow powder (yield 68.5% over two steps). ^{1}H NMR (400 MHz, CD_3OD) δ 7.42 (d, J = 8.9 Hz, 2H), 7.31 (ddd, J = 15.0, 8.3, 1.9 Hz, 1H), 6.96 (d, J = 8.9 Hz, 2H), 6.89–6.78 (m, 2H), 6.05 (d, J = 15.0 Hz, 1H), 3.30 (d, J = 7.3, 5.9 Hz, 2H), 3.22 (dd, J = 6.1, 4.0 Hz, 4H), 2.99 (dd, J = 6.1, 4.0 Hz, 4H), 1.19 (t, J = 7.3 Hz, 3H). ^{13}C NMR (101 MHz, CD_3OD) δ 161.48, 138.15, 137.55, 131.51, 129.24, 126.18, 124.61, 116.74, 116.64, 50.43, 50.26, 46.46, 46.44, 35.31, 14.80. Exact mass calcd for C17H23N3O $[M+Na]^+$: 308.1739; found 308.1740.

4.1.16. (2E,4E)-5-(4-morpholinophenyl)-1-(piperidin-1-yl)penta-2,4-dien-1-one (**3k**)

2a was reacted with 4-(4-formylphenyl)morpholine following

the general procedure B to give the desired product **3k** as a light yellow powder (88.0%). ^{1}H NMR (400 MHz, $CDCl_3$) δ 7.42 (ddd, J = 14.6, 6.0, 4.3 Hz, 1H), 7.37 (d, J = 8.8 Hz, 2H), 6.87 (d, J = 8.6 Hz, 2H), 6.80–6.74 (m, 2H), 6.41 (d, J = 14.6 Hz, 1H), 3.91–3.81 (m, 4H), 3.58 (d, J = 37.6 Hz, 4H), 3.24–3.16 (m, 4H), 1.66 (dd, J = 11.0, 6.1 Hz, 2H), 1.58 (dt, J = 10.9, 5.5 Hz, 4H). ^{13}C NMR (101 MHz, $CDCl_3$) δ 165.73, 151.32, 143.09, 138.52, 130.63, 128.26, 124.53, 119.32, 115.35, 66.84, 48.82, 47.03, 43.36, 26.87, 25.80, 24.82. Exact mass calcd for C20H26N2O2 [M+Na]$^+$: 349.1892; found 349.1890.

4.1.17. (2E,4E)-1-(piperidin-1-yl)-5-(4-(piperidin-1-yl)phenyl) penta-2,4-dien-1-one (**3l**)

2a was reacted with 4-piperidinobenzaldehyde following the general procedure B to give the desired product **3l** as a light yellow powder (78.6%). ^{1}H NMR (400 MHz, $CDCl_3$) δ 7.43 (ddd, J = 14.6, 8.5, 1.8 Hz, 1H), 7.33 (d, J = 8.8 Hz, 2H), 6.87 (d, J = 8.5 Hz, 2H), 6.81–6.70 (m, 2H), 6.39 (d, J = 14.6 Hz, 1H), 3.58 (d, J = 36.0 Hz, 4H), 3.28–3.15 (m, 4H), 1.75–1.54 (m, 12H). ^{13}C NMR (101 MHz, $CDCl_3$) δ 165.87, 152.17, 143.41, 138.99, 128.26, 126.92, 123.77, 118.71, 115.69, 49.86, 25.73, 24.86, 24.47. Exact mass calcd for C21H28N2O [M+Na]$^+$: 347.2099; found 347.2101.

4.1.18. (2E,4E)-5-(4-chlorophenyl)-1-(piperidin-1-yl)penta-2,4-dien-1-one (**3m**)

2a was reacted with 4-chlorobenzaldehyde following the general procedure B to give the desired product **3m** as a white powder (68.2%). ^{1}H NMR (400 MHz, DMSO-d_6) δ 7.56 (d, J = 8.5 Hz, 2H), 7.45 (d, J = 8.5 Hz, 2H), 7.25 (dd, J = 14.4, 10.9 Hz, 1H), 7.13 (dd, J = 15.5, 10.9 Hz, 1H), 6.97 (d, J = 15.5 Hz, 1H), 6.80 (d, J = 14.4 Hz, 1H), 3.54 (s, 4H), 1.63 (dt, J = 11.2, 5.6 Hz, 2H), 1.50 (s, 4H). ^{13}C NMR (101 MHz, DMSO-d_6) δ 164.04, 141.12, 136.14, 135.28, 132.79, 128.82, 128.41, 128.23, 122.44, 46.09, 42.46, 26.44, 25.36, 24.11. Exact mass calcd for C16H18ClNO [M+Na]$^+$: 298.0975; found 298.0976.

4.1.19. (2E,4E)-5-(benzo[d][1,3]dioxol-5-yl)-1-(piperidin-1-yl) penta-2,4-dien-1-one (**3n**)

2a was reacted with piperonyl aldehyde following the general procedure B to give the desired product **3n** as a white powder (75.3%). ^{1}H NMR (400 MHz, DMSO-d_6) δ 7.21 (dd, J = 14.5, 10.5 Hz, 1H), 7.16 (d, J = 1.2 Hz, 1H), 6.95 (dt, J = 20.7, 8.3 Hz, 3H), 6.86 (d, J = 15.6 Hz, 1H), 6.67 (d, J = 14.5 Hz, 1H), 6.04 (s, 2H), 3.51 (s, 4H), 1.65–1.55 (m, 2H), 1.47 (s, 4H). ^{13}C NMR (101 MHz, DMSO-d_6) δ 164.20, 147.91, 147.71, 141.71, 137.57, 130.83, 125.66, 122.41, 120.76, 108.48, 105.45, 101.25, 46.06, 42.42, 26.44, 25.41, 24.13. Exact mass calcd for C17H19NO3 [M+Na]$^+$: 308.1263; found 308.1264.

4.1.20. (2E,4E)-5-(benzo[d][1,3]dioxol-5-yl)-N,N-diethylpenta-2,4-dienamide (**3o**)

2b was reacted with piperonyl aldehyde following the general procedure B to give the desired product **3o** as a white powder (75.8%). ^{1}H NMR (400 MHz, $CDCl_3$) δ 7.44 (ddd, J = 14.6, 7.4, 2.6 Hz, 1H), 6.99 (d, J = 1.5 Hz, 1H), 6.89 (dd, J = 8.0, 1.5 Hz, 1H), 6.77 (d, J = 8.5 Hz, 2H), 6.75 (d, J = 5.0 Hz, 1H), 6.36 (d, J = 14.6 Hz, 1H), 5.97 (s, 2H), 3.53–3.34 (m, 4H), 1.23 (t, J = 7.1 Hz, 3H), 1.17 (t, J = 6.5 Hz, 3H). ^{13}C NMR (101 MHz, $CDCl_3$) δ 165.88, 148.21, 148.14, 142.50, 138.44, 131.05, 125.36, 122.53, 120.27, 108.50, 105.71, 101.28, 42.22, 40.98, 15.03, 13.26. Exact mass calcd for C16H19NO3 [M+Na]$^+$: 296.1263; found 296.1265.

4.1.21. (2E,4E)-5-(benzo[d][1,3]dioxol-5-yl)-N-ethylpenta-2,4-dienamide (**3p**)

2c was reacted with piperonyl aldehyde following the general procedure B to give the desired product **3p** as a white powder (78.2%). ^{1}H NMR (400 MHz, DMSO-d_6) δ 8.03 (t, J = 5.4 Hz, 1H), 7.26 (d, J = 1.5 Hz, 1H), 7.15 (dd, J = 15.0, 10.2 Hz, 1H), 7.00 (dd, J = 8.1, 1.5 Hz, 1H), 6.97–6.88 (m, 2H), 6.85 (d, J = 15.5 Hz, 1H), 6.07 (d, J = 15.0 Hz, 1H), 6.05 (s, 2H), 3.21–3.12 (m, 2H), 1.06 (t, J = 7.2 Hz, 3H). ^{13}C NMR (101 MHz, DMSO-d_6) δ 164.89, 147.90, 147.65, 139.05, 137.68, 130.86, 125.27, 124.67, 122.57, 108.40, 105.60, 101.22, 33.40, 14.75. Exact mass calcd for C14H15NO3 [M+Na]$^+$: 268.0950; found 268.0952.

4.1.22. (2E,4E)-5-(furan-2-yl)-1-(piperidin-1-yl)penta-2,4-dien-1-one (**3q**)

2a was reacted with 2-furanaldehyde following the general procedure B to give the desired product **3q** as a light yellow powder (64.5%). ^{1}H NMR (400 MHz, $CDCl_3$) δ 7.39 (s, 1H), 7.39–7.31 (m, 1H), 6.79 (dd, J = 15.4, 11.3 Hz, 1H), 6.60 (d, J = 15.4 Hz, 1H), 6.44 (d, J = 14.6 Hz, 1H), 6.42–6.36 (m, 2H), 3.56 (d, J = 44.1 Hz, 4H), 1.68–1.61 (m, 2H), 1.57 (d, J = 4.3 Hz, 4H). ^{13}C NMR (101 MHz, $CDCl_3$) δ 165.45, 152.62, 143.22, 142.03, 125.55, 125.43, 120.85, 112.06, 110.92, 47.02, 43.37, 26.83, 25.72, 24.74. Exact mass calcd for C14H17NO2 [M+Na]$^+$: 254.1157; found 254.1159.

4.1.23. (2E,4E)-1-(piperidin-1-yl)-5-(thiophen-2-yl)penta-2,4-dien-1-one (**3r**)

2a was reacted with 2-thiophenaldehyde following the general procedure B to give the desired product **3r** as a light yellow powder (67.8%). ^{1}H NMR (400 MHz, $CDCl_3$) δ 7.37 (dd, J = 14.6, 11.1 Hz, 1H), 7.22 (d, J = 5.1 Hz, 1H), 7.06 (d, J = 3.6 Hz, 1H), 6.98 (dd, J = 5.1, 3.6 Hz, 1H), 6.95 (d, J = 15.8 Hz, 1H), 6.69 (dd, J = 15.3, 11.1 Hz, 1H), 6.44 (d, J = 14.6 Hz, 1H), 3.56 (s, 3H), 1.68–1.62 (m, 2H), 1.57 (dt, J = 11.0, 5.5 Hz, 4H). ^{13}C NMR (101 MHz, $CDCl_3$) δ 165.37, 142.02, 142.00, 131.15, 127.94, 127.86, 126.78, 125.97, 120.60, 46.95, 43.56, 26.20, 24.75. Exact mass calcd for C14H17NOS [M+H]$^+$: 248.1109; found 248.1104.

4.1.24. (2E,4E)-N,N-diethyl-5-(thiophen-2-yl)penta-2,4-dienamide (**3s**)

2b was reacted with 2-thiophenaldehyde following the general procedure B to give the desired product **3s** as a light yellow powder (56.3%). ^{1}H NMR (400 MHz, DMSO-d_6) δ 7.57 (d, J = 5.1 Hz, 1H), 7.28 (d, J = 3.6 Hz, 1H), 7.20–7.15 (m, 1H), 7.15–7.11 (m, 1H), 7.09 (dd, J = 5.1, 3.6 Hz, 1H), 6.73 (dd, J = 15.4, 11.1 Hz, 1H), 6.06 (d, J = 15.1 Hz, 1H), 3.55–3.34 (m, 4H), 1.24 (t, J = 7.1 Hz, 3H), 1.18 (t, J = 6.5 Hz, 3H). ^{13}C NMR (101 MHz, DMSO-d_6) δ 165.06, 141.05, 138.21, 130.47, 128.19, 127.81, 126.68, 126.09, 125.12, 42.12, 40.89, 15.03, 13.16. Exact mass calcd for C11H13NOS [M+Na]$^+$: 258.0929; found 258.0928.

4.1.25. (2E,4E)-N-ethyl-5-(thiophen-2-yl)penta-2,4-dienamide (**3t**)

2d was reacted with 2-thiophenaldehyde following the general procedure B to give the desired product **3t** as a light yellow powder (63.3%). ^{1}H NMR (400 MHz, DMSO-d_6) δ 8.04 (t, J = 5.3 Hz, 1H), 7.55 (d, J = 5.1 Hz, 1H), 7.26 (d, J = 3.6 Hz, 1H), 7.20–7.15 (m, 1H), 7.15–7.11 (m, 1H), 7.09 (dd, J = 5.1, 3.6 Hz, 1H), 6.73 (dd, J = 15.4, 11.1 Hz, 1H), 6.09 (d, J = 15.1 Hz, 1H), 3.17 (qd, J = 7.2, 5.8 Hz, 2H), 1.06 (t, J = 7.2 Hz, 3H). ^{13}C NMR (101 MHz, DMSO-d_6) δ 164.76, 141.35, 138.36, 130.66, 128.19, 127.99, 126.79, 126.18, 125.22, 33.42, 14.74. Exact mass calcd for C11H13NOS [M+Na]$^+$: 230.0616; found 230.0617.

4.1.26. (2E,4E)-1-(piperidin-1-yl)-5-(thiophen-3-yl)penta-2,4-dien-1-one (**3u**)

2a was reacted with 3-thiophenaldehyde following the general procedure B to give the desired product **3u** as a light yellow powder (65.4%). ^{1}H NMR (400 MHz, $CDCl_3$) δ 7.40 (dd, J = 14.6, 10.9 Hz, 1H), 7.32–7.24 (m, 3H), 6.86 (d, J = 15.5 Hz, 1H), 6.73 (dd, J = 15.5, 10.9 Hz, 1H), 6.45 (d, J = 14.6 Hz, 1H), 3.58 (m, 4H), 1.68 (m, 2H), 1.59 (m, 4H). ^{13}C NMR (101 MHz, $CDCl_3$) δ 165.53, 142.65, 139.61, 132.51,

127.19, 126.57, 125.02, 124.43, 120.50, 26.35, 24.80. Exact mass calcd for C14H17NOS $[M+H]^+$: 248.1109; found 248.1080.

4.1.27. (2E,4E)-5-(1-methyl-1H-pyrrol-2-yl)-1-(piperidin-1-yl) penta-2,4-dien-1-one (**3v**)

2a was reacted with 1-methyl-2-pyrrolecarboxaldehyde following the general procedure B to give the desired product **3v** as a white powder (68.3%). ^{1}H NMR (400 MHz, $CDCl_3$) δ 7.43 (dd, J = 14.5, 10.5 Hz, 1H), 6.73 (d, J = 15.3 Hz, 1H), 6.67 (d, J = 10.5 Hz, 1H), 6.65 (d, J = 2.5 Hz, 1H), 6.51 (dd, J = 3.8, 1.5 Hz, 1H), 6.37 (d, J = 14.5 Hz, 1H), 6.14 (dd, J = 3.6, 2.8 Hz, 1H), 3.65 (s, 1H), 3.61–3.54 (m, 2H), 1.71–1.63 (m, 1H), 1.59 (dt, J = 10.9, 5.4 Hz, 2H). ^{13}C NMR (101 MHz, $CDCl_3$) δ 165.78, 143.33, 131.39, 126.68, 125.03, 123.92, 118.44, 108.96, 108.65, 34.21, 24.84, 24.58. Exact mass calcd for C15H20N2O $[M+H]^+$: 245.1654; found 245.1647.

4.1.28. (2E,4E)-5-(5-methoxy-1-methyl-1H-indol-3-yl)-1-(piperidin-1-yl)penta-2,4-dien-1-one (**3w**)

2a was reacted with 1-isopropyl-5-methoxy-3-indolecarboxaldehyde following the general procedure B to give the desired product **3w** as a white powder (45.3%). ^{1}H NMR (400 MHz, $CDCl_3$) δ 7.56 (dd, J = 14.6, 11.1 Hz, 1H), 7.33 (d, J = 2.3 Hz, 1H), 7.23–7.20 (m, 2H), 7.06 (d, J = 15.5 Hz, 1H), 6.94 (dd, J = 8.9, 2.4 Hz, 1H), 6.83 (dd, J = 15.5, 11.1 Hz, 1H), 6.36 (d, J = 14.6 Hz, 1H), 3.91 (s, 3H), 3.77 (s, 3H), 3.64–3.59 (m, 4H), 1.71–1.65 (m, 2H), 1.62 (m, 4H). ^{13}C NMR (101 MHz, DMSO-d_6) δ 164.73, 154.53, 143.78, 132.76, 132.21, 131.88, 125.96, 121.92, 117.00, 112.22, 111.70, 111.10, 102.41, 55.64, 46.03, 42.38, 32.81, 26.53, 25.46, 24.22. Exact mass calcd for C20H24N2O2 $[M+Na]^+$: 347.1735; found 347.1736.

4.1.29. General procedure C for the synthesis of **4**

1 M boron tribromide (BBr_3) in DCM (2.66 mL, 2.66 mmol) was added to a solution of compound **3a** (0.2 g, 0.50 mmol) in dry DCM (20 mL) at −78 °C and stirred for 2 h. The reaction mixture was allowed to raise to room temperature slowly and stirred for another 4 h, as indicated by TLC. The reaction was carefully mixed with saturated aqueous $NaHCO_3$ (30 mL) at 0 °C and stirred for 30 min. This mixture was extracted with ethyl acetate twice (20 mL × 2), and the organic portion was combined, further washed with brine, and dried with $MgSO_4$. The residue was filtered, concentrated, and purified by silica gel column chromatography to yield **4**.

4.1.30. (2E,4E)-5-(4-hydroxyphenyl)-1-(piperidin-1-yl)penta-2,4-dien-1-one (**4a**)

3a was demethylated with BBr_3 following the general procedure C to give the desired product **4a** as a light brown yellow powder (98.0%). ^{1}H NMR (400 MHz, $CDCl_3$) δ 7.46–7.37 (m, 1H), 7.30 (d, J = 8.4 Hz, 2H), 6.86 (d, J = 8.4 Hz, 2H), 6.74 (m, 2H), 6.40 (d, J = 14.4 Hz, 1H), 3.60 (s, 4H), 1.72–1.63 (m, 2H), 1.60 (s, 4H). ^{13}C NMR (101 MHz, $CDCl_3$) δ 166.12, 157.12, 143.73, 139.18, 128.76, 128.63, 124.35, 118.75, 115.93, 100.00, 27.10, 26.35, 24.58. Exact mass calcd for C16H19NO2 $[M+Na]^+$: 280.1313; found 280.1314.

4.1.31. (2E,4E)-5-(3-hydroxyphenyl)-1-(piperidin-1-yl)penta-2,4-dien-1-one (**4b**)

3b was demethylated with BBr_3 following the general procedure C to give the desired product **4b** as a light brown yellow powder (23.1%). ^{1}H NMR (400 MHz, DMSO-d_6) δ 9.88 (s, 1H), 7.44 (d, J = 6.7 Hz, 1H), 7.22 (ddd, J = 14.4, 8.4, 2.1 Hz, 1H), 7.17–7.03 (m, 3H), 6.86 (d, J = 7.8 Hz, 1H), 6.80 (t, J = 7.4 Hz, 1H), 6.70 (d, J = 14.4 Hz, 1H), 3.52 (s, 4H), 1.65–1.55 (m, 2H), 1.48 (s, 4H). ^{13}C NMR (101 MHz, DMSO-d_6) δ 164.31, 155.49, 142.52, 133.51, 129.53, 127.26, 127.13, 123.04, 120.71, 119.30, 115.94, 46.04, 42.43, 26.48, 25.40, 24.16. Exact mass calcd for C16H19NO2 $[M+Na]^+$: 280.1313; found 280.1314.

4.1.32. (2E,4E)-5-(2-hydroxyphenyl)-1-(piperidin-1-yl)penta-2,4-dien-1-one (**4c**)

3c was demethylated with BBr_3 following the general procedure C to give the desired product **4c** as a light brown yellow powder (48.2%). ^{1}H NMR (400 MHz, CD_3OD) δ 7.33 (dd, J = 14.7, 10.9 Hz, 1H), 7.16 (t, J = 7.9 Hz, 1H), 7.03–6.91 (m, 3H), 6.83 (d, J = 15.6 Hz, 1H), 6.73 (dd, J = 8.0, 2.0 Hz, 1H), 6.66 (d, J = 14.7 Hz, 1H), 3.67–3.56 (m, 4H), 1.69 (dd, J = 10.5, 5.5 Hz, 2H), 1.59 (s, 4H). ^{13}C NMR (101 MHz, CD_3OD) δ 167.62, 158.88, 144.26, 140.43, 139.20, 130.77, 128.02, 121.54, 119.77, 116.93, 114.43, 48.14, 44.54, 27.86, 26.87, 25.53. Exact mass calcd for C16H19NO2 $[M+Na]^+$: 280.1313; found 280.1314.

4.1.33. (2E,4E)-N,N-diethyl-5-(4-hydroxyphenyl)penta-2,4-dienamide (**4d**)

2b was reacted with 4-methoxybenzaldehyde following the general procedure B to give an intermediate without further purification and then demethlyated with BBr_3 following the general procedure C to give the desired product **4d** as a light yellow powder (69.5% over two steps). ^{1}H NMR (400 MHz, DMSO-d_6) δ 8.02 (dd, J = 15.9, 11.2 Hz, 1H), 7.30 (d, J = 8.5 Hz, 2H), 6.80 (d, J = 8.5 Hz, 2H), 6.64 (d, J = 15.9 Hz, 1H), 6.45 (t, J = 11.2 Hz, 1H), 5.59 (d, J = 11.2 Hz, 1H), 2.75 (q, J = 7.2 Hz, 4H), 1.11 (t, J = 7.2 Hz, 6H). ^{13}C NMR (101 MHz, DMSO-d_6) δ 169.84, 158.33, 138.98, 136.85, 128.14, 127.55, 123.84, 123.09, 115.77, 41.74, 12.45. Exact mass calcd for C15H17NO2 $[M+Na]^+$: 268.1313; found 268.1316.

4.1.34. (2E,4E)-N-ethyl-5-(4-hydroxyphenyl)penta-2,4-dienamide (**4e**)

2c was reacted with 4-methoxybenzaldehyde following the general procedure B to give an intermediate without further purification and then demethlyated with BBr_3 following the general procedure C to give the desired product **4e** as a light yellow powder (65.3% over two steps). ^{1}H NMR (400 MHz, DMSO-d_6) δ 8.11 (dd, J = 15.9, 11.1 Hz, 1H), 7.29 (d, J = 8.4 Hz, 2H), 6.84 (d, J = 8.4 Hz, 2H), 6.58 (d, J = 15.9 Hz, 1H), 6.35 (t, J = 11.1 Hz, 1H), 5.59 (d, J = 11.1 Hz, 1H), 2.79 (q, J = 7.2 Hz, 2H), 1.13 (t, J = 7.2 Hz, 3H). ^{13}C NMR (101 MHz, DMSO-d_6) δ 170.69, 158.54, 137.07, 135.54, 127.90, 127.55, 126.30, 123.50, 115.82, 34.16, 13.63. Exact mass calcd for C13H15NO2 $[M+Na]^+$: 240.1000; found 240.1001.

4.1.35. General procedure D for the synthesis of **6**

Malonic acid (0.3 g, 2.86 mmol) was added to the stirred solution of the corresponding aldehyde **5** (1.3 mmol) in pyridine (15 mL) and piperidine (1.5 mL). The mixture was heated to reflux for 8 h. The reaction mixture was neutralized with hydrochloric acid in an ice bath. The precipitates were filtered and washed with cold water. The crude product was then recrystallized from ethanol to afford the corresponding acids **6**.

4.1.36. (E)-3-(4-(4-(tert-butoxycarbonyl)piperazin-1-yl)phenyl) acrylic acid (**6a**)

Malonic acid was reacted with *tert*-butyl 4-(4-formylphenyl) tetrahydro-1(2*H*)-pyrazinecarboxylate following the general procedure D to give the desired product **6a** as a light yellow powder (67.1%). ^{1}H NMR (400 MHz, DMSO-d_6) δ 12.06 (s, 1H), 7.53 (d, J = 8.8 Hz, 2H), 7.48 (d, J = 15.9 Hz, 1H), 6.95 (d, J = 8.8 Hz, 2H), 6.29 (d, J = 15.9 Hz, 1H), 3.50–3.38 (m, 4H), 3.28–3.13 (m, 4H), 1.42 (s, 9H). Exact mass calcd for C18H24N2O4 $[M-H]^-$: 331.1663; found 331.1664.

4.1.37. (E)-3-(4-(pyrrolidin-1-yl)phenyl)acrylic acid (**6b**)

Malonic acid was reacted with 1-(4-formylphenyl)pyrrolidine following the general procedure D to give the desired product **6b** as a light yellow powder (77.1%). ^{1}H NMR (400 MHz, DMSO-d_6) δ 7.52–7.39 (m, 3H), 6.53 (d, J = 8.7 Hz, 2H), 6.17 (d, J = 15.9 Hz, 1H),

3.28 (t, J = 6.5 Hz, 4H), 2.00−1.90 (m, 4H). Exact mass calcd for C13H15NO2 [M-H]$^-$: 216.1030; found 216.1031.

*4.1.38. (E)-3-(benzo[d][1,3]dioxol-5-yl)acrylic acid (**6c**)*

Malonic acid was reacted with piperonyl aldehyde following the general procedure D to give the desired product **6c** as a light yellow powder (69.5%). ^{1}H NMR (400 MHz, DMSO-d_6) δ 7.50 (d, J = 15.9 Hz, 1H), 7.36 (d, J = 1.5 Hz, 1H), 7.15 (dd, J = 8.1, 1.5 Hz, 1H), 6.94 (d, J = 8.1 Hz, 1H), 6.39 (d, J = 15.9 Hz, 1H), 6.07 (s, 2H). Exact mass calcd for C10H8O4 [M-H]$^-$: 191.0350; found 191.0351.

*4.1.39. (E)-3-(2-methoxyphenyl)acrylic acid (**6d**)*

Malonic acid was reacted with 2-methoxybenzaldehyde following the general procedure D to give the desired product **6d** as a light yellow powder (75.6%). ^{1}H NMR (400 MHz, $CDCl_3$) δ 8.10 (d, J = 16.1 Hz, 1H), 7.54 (dd, J = 7.7, 1.4 Hz, 1H), 7.41−7.34 (m, 1H), 6.98 (t, J = 7.5 Hz, 1H), 6.93 (d, J = 8.3 Hz, 1H), 6.56 (d, J = 16.1 Hz, 1H), 3.90 (s, 3H). Exact mass calcd for C10H10O3 [M+H]$^+$: 179.0708; found 179.0702.

*4.1.40. (E)-3-(thiophen-2-yl)acrylic acid (**6e**)*

Malonic acid was reacted with 2-thenaldehyde following the general procedure D to give the desired product **6e** as a light yellow powder (65.5%). ^{1}H NMR (400 MHz, DMSO-d_6) δ 12.35 (s, 1H), 7.74 (d, J = 15.8 Hz, 1H), 7.70 (d, J = 5.0 Hz, 1H), 7.50 (d, J = 3.4 Hz, 1H), 7.14 (dd, J = 5.0, 3.7 Hz, 1H), 6.17 (d, J = 15.8 Hz, 1H). Exact mass calcd for C7H6O2S [M-H]$^-$: 153.0016; found 153.0016.

*4.1.41. General procedure E for the synthesis of **7***

6 (1 mmol) was dissolved into 2 mL DMF. *O*-(7-aza-1*H*-benzotriazole-1-yl)-*N*,*N*,*N*′,*N*′-tetramethyluronium hexafluorophosphate (HATU) (1.5 mmol) was added to a solution, followed by corresponding lamins (1.2 mmol), triethylamine (3.0 mmol). The mixture was reacted at room temperature for 4 h. After the reaction was completed, 8 mL water was added to quench the reaction. Then exacted with ethyl acetate 2 mL (three times). The organic layer was dried over anhyd. Na_2SO_4 and concentrated under reduced pressure. The obtained crude product was purified by silico column chromatography to get pure product **7**.

*4.1.42. (E)-3-(4-(piperazin-1-yl)phenyl)-1-(piperidin-1-yl)prop-2-en-1-one (**7a**)*

6a was reacted with piperidine following the general procedure E to give an intermediate, which was then added to a solution of trifluoroacetic acid (2 mL) at 0 °C. The reaction mixture was then allowed to warm to room temperature and stirred for 1 h until completed, as indicated by TLC. Then trifluoroacetic acid was evaporated under reduced pressure. The residue was dissolved with ethyl acetate (10 mL), and washed with saturated aqueous $NaHCO_3$ (10 mL × 2), dried over anhyd. Na_2SO_4 and concentrated under reduced pressure. The obtained crude product was purified by column chromatography to get pure product **7a** as yellow powder with a yield of 76.4% over two steps. ^{1}H NMR (400 MHz, $CDCl_3$) δ 7.56 (d, J = 15.4 Hz, 1H), 7.44 (d, J = 8.7 Hz, 2H), 6.86 (d, J = 8.7 Hz, 2H), 6.77 (d, J = 15.4 Hz, 1H), 3.61 (d, J = 19.9 Hz, 4H), 3.49−3.36 (m, 4H), 3.34−3.16 (m, 4H), 1.72−1.64 (m, 2H), 1.60 (d, J = 4.1 Hz, 4H). ^{13}C NMR (101 MHz, $CDCl_3$) δ 165.71, 150.99, 141.74, 129.11, 127.96, 116.23, 115.19, 47.03, 46.82, 43.77, 43.38, 26.76, 25.64, 24.66. Exact mass calcd for C18H25N3O [M+H]$^+$: 300.2076; found 300.2076.

*4.1.43. (E)-N,N-diethyl-3-(4-(piperazin-1-yl)phenyl)acrylamide (**7b**)*

6a was reacted with diethylamine following the general procedure E to give an intermediate, which was then added to a solution of trifluoroacetic acid (2 mL) at 0 °C. The reaction mixture was then allowed to warm to room temperature and stirred for 1 h until completed, as indicated by TLC. Then trifluoroacetic acid was evaporated under reduced pressure. The residue was dissolved with ethyl acetate (10 mL), and washed with saturated aqueous $NaHCO_3$ (10 mL × 2), dried over anhyd. Na_2SO_4 and concentrated under reduced pressure. The obtained crude product was purified by column chromatography to get pure product **7b** as yellow powder with a yield of 79.8% over two steps. ^{1}H NMR (400 MHz, $CDCl_3$) δ 7.64 (d, J = 15.3 Hz, 1H), 7.44 (d, J = 8.7 Hz, 2H), 6.88 (d, J = 8.7 Hz, 2H), 6.67 (d, J = 15.3 Hz, 1H), 3.48 (d, J = 2.6 Hz, 4H), 3.35−3.19 (m, 4H), 3.08 (dd, J = 6.0, 4.0 Hz, 4H), 1.26 (s, 6H). ^{13}C NMR (101 MHz, $CDCl_3$) δ 166.21, 152.17, 142.17, 129.08, 126.67, 115.38, 114.36, 48.94, 45.56, 42.26, 41.09, 29.70, 15.06. Exact mass calcd for C17H25N3O [M+H]$^+$: 288.2076; found 288.2077.

*4.1.44. (E)-N-ethyl-3-(4-(piperazin-1-yl)phenyl)acrylamide (**7c**)*

6a was reacted with ethylamine following the general procedure E to give an intermediate, which was then added to a solution of trifluoroacetic acid (2 mL) at 0 °C. The reaction mixture was then allowed to warm to room temperature and stirred for 1 h until completed, as indicated by TLC. Then trifluoroacetic acid was evaporated under reduced pressure. The residue was dissolved with ethyl acetate (10 mL), and washed with saturated aqueous $NaHCO_3$ (10 mL × 2), dried over anhyd. Na_2SO_4 and concentrated under reduced pressure. The obtained crude product was purified by column chromatography to get pure product **7c** as yellow powder with a yield of 65.4% over two steps. ^{1}H NMR (400 MHz, $CDCl_3$) δ 7.54 (d, J = 15.5 Hz, 1H), 7.40 (d, J = 8.8 Hz, 2H), 6.86 (d, J = 8.8 Hz, 2H), 6.21 (d, J = 15.5 Hz, 1H), 5.55 (s, 1H), 3.46−3.35 (m, 2H), 3.27−3.16 (m, 4H), 3.07−2.97 (m, 4H), 1.20 (t, J = 7.3 Hz, 3H). ^{13}C NMR (101 MHz, $CDCl_3$) δ 166.54, 152.62, 140.82, 129.20, 125.80, 117.32, 115.29, 49.43, 46.05, 34.68, 15.11. Exact mass calcd for C15H21N3O [M+Na]$^+$: 260.1763; found 260.1762.

*4.1.45. (E)-1-(piperidin-1-yl)-3-(4-(pyrrolidin-1-yl)phenyl)prop-2-en-1-one (**7d**)*

6b was reacted with piperidine following the general procedure E to give the desired product **7d** as a light yellow powder (75.3%). ^{1}H NMR (400 MHz, $CDCl_3$) δ 7.61 (d, J = 15.2 Hz, 1H), 7.41 (d, J = 8.7 Hz, 2H), 6.67 (d, J = 15.2 Hz, 1H), 6.52 (d, J = 8.7 Hz, 2H), 3.62 (s, 4H), 3.32 (t, J = 6.6 Hz, 4H), 2.04−1.97 (m, 4H), 1.71−1.63 (m, 2H), 1.60 (d, J = 4.6 Hz, 4H). ^{13}C NMR (101 MHz, $CDCl_3$) δ 166.30, 148.76, 143.11, 129.37, 122.73, 111.55, 111.49, 47.55, 46.85, 43.37, 26.72, 25.46, 24.78. Exact mass calcd for C18H24N2O [M+Na]$^+$: 307.1786; found 307.1784.

*4.1.46. (E)-N,N-diethyl-3-(4-(pyrrolidin-1-yl)phenyl)acrylamide (**7e**)*

6b was reacted with diethylamine following the general procedure E to give the desired product **7e** as a light yellow powder (68.9%). ^{1}H NMR (400 MHz, $CDCl_3$) δ 7.64 (d, J = 15.2 Hz, 1H), 7.40 (d, J = 8.7 Hz, 2H), 6.58 (d, J = 15.2 Hz, 1H), 6.51 (d, J = 8.7 Hz, 2H), 3.55−3.39 (m, 4H), 3.30 (t, J = 6.6 Hz, 4H), 2.10−1.92 (m, 4H), 1.32−1.10 (m, 6H). ^{13}C NMR (101 MHz, $CDCl_3$) δ 166.73, 148.88, 143.15, 129.51, 122.77, 111.77, 111.64, 47.63, 42.31, 41.11, 25.54, 15.13, 13.43. Exact mass calcd for C17H24N2O [M+Na]$^+$: 295.1786; found 295.1792.

*4.1.47. (E)-3-(benzo[d][1,3]dioxol-5-yl)-1-(piperidin-1-yl)prop-2-en-1-one (**7f**)*

6c was reacted with piperidine following the general procedure E to give the desired product **7f** as a light yellow powder (52.9%). ^{1}H NMR (400 MHz, $CDCl_3$) δ 7.56 (d, J = 15.3 Hz, 1H), 7.03 (d, J = 1.4 Hz, 1H), 6.99 (dd, J = 8.0, 1.4 Hz, 1H), 6.79 (d, J = 8.0 Hz, 1H), 6.73 (d,

J = 15.3 Hz, 1H), 5.98 (s, 2H), 3.61 (s, 4H), 1.71–1.64 (m, 2H), 1.64–1.56 (m, 4H). ^{13}C NMR (101 MHz, $CDCl_3$) δ 165.62, 148.98, 148.34, 142.13, 130.10, 123.74, 115.86, 108.63, 106.50, 101.53, 26.22, 24.81. Exact mass calcd for C15H17NO3 $[M+Na]^+$: 282.1106; found 282.1105.

*4.1.48. (E)-3-(benzo[d][1,3]dioxol-5-yl)-N,N-diethylacrylamide (**7g**)*

6c was reacted with diethylamine following the general procedure E to give the desired product **7g** as a light yellow powder (82.7%). ^{1}H NMR (400 MHz, $CDCl_3$) δ 7.62 (d, *J* = 15.3 Hz, 1H), 7.03 (d, *J* = 1.6 Hz, 1H), 7.00 (dd, *J* = 8.0, 1.6 Hz, 1H), 6.80 (d, *J* = 8.0 Hz, 1H), 6.65 (d, *J* = 15.3 Hz, 1H), 5.99 (s, 2H), 3.47 (s, 4H), 1.25 (t, *J* = 6.5 Hz, 3H), 1.18 (t, *J* = 6.5 Hz, 3H). ^{13}C NMR (101 MHz, $CDCl_3$) δ 166.01, 149.00, 148.32, 142.18, 130.08, 123.83, 115.97, 108.65, 106.51, 101.53, 42.41, 41.22, 15.22, 13.39. Exact mass calcd for C14H17NO3 $[M+Na]^+$: 270.1106; found 270.1107.

*4.1.49. (E)-3-(benzo[d][1,3]dioxol-5-yl)-N-ethylacrylamide (**7h**)*

6c was reacted with ethylamine following the general procedure E to give the desired product **7h** as a light yellow powder (73.7%). ^{1}H NMR (400 MHz, $CDCl_3$) δ 7.52 (d, *J* = 15.5 Hz, 1H), 6.98 (d, *J* = 1.5 Hz, 1H), 6.96 (dd, *J* = 8.0, 1.5 Hz, 1H), 6.78 (d, *J* = 8.0 Hz, 1H), 6.21 (d, *J* = 15.5 Hz, 1H), 5.70 (s, 1H), 3.41 (qd, *J* = 7.3, 5.9 Hz, 2H), 1.20 (t, *J* = 7.3 Hz, 3H). ^{13}C NMR (101 MHz, $CDCl_3$) δ 166.08, 149.11, 148.34, 140.65, 129.45, 123.88, 118.99, 108.65, 106.45, 101.54, 34.73, 15.05. Exact mass calcd for C12H13NO3 $[M+Na]^+$: 242.0793; found 242.0787.

*4.1.50. (E)-3-(2-methoxyphenyl)-1-(piperidin-1-yl)prop-2-en-1-one (**7i**)*

6d was reacted with piperidine following the general procedure E to give the desired product **7i** as a light yellow powder (84.5%). ^{1}H NMR (400 MHz, $CDCl_3$) δ 7.89 (d, *J* = 15.6 Hz, 1H), 7.48 (dd, *J* = 7.6, 1.5 Hz, 1H), 7.33–7.27 (m, 1H), 6.99 (d, *J* = 15.6 Hz, 1H), 6.94 (t, *J* = 7.8 Hz, 1H), 6.90 (d, *J* = 8.3 Hz, 1H), 3.87 (s, 3H), 3.61 (s, 4H), 1.72–1.64 (m, 2H), 1.63–1.55 (m, 4H). ^{13}C NMR (101 MHz, $CDCl_3$) δ 166.15, 158.22, 137.69, 130.55, 128.90, 124.77, 120.72, 118.90, 111.25, 55.62, 47.14, 43.43, 26.87, 25.83, 24.84. Exact mass calcd for C15H19NO2 $[M+H]^+$: 246.1494; found 246.1495.

*4.1.51. (E)-N,N-diethyl-3-(2-methoxyphenyl)acrylamide (**7j**)*

6d was reacted with piperidine following the general procedure E to give the desired product **7j** as a light yellow powder (83.6%). ^{1}H NMR (400 MHz, $CDCl_3$) δ 7.94 (d, *J* = 15.6 Hz, 1H), 7.48 (dd, *J* = 7.6, 1.5 Hz, 1H), 7.33–7.27 (m, 1H), 6.98–6.88 (m, 3H), 3.86 (s, 3H), 3.47 (q, *J* = 7.1 Hz, 4H), 1.21 (s, 6H). ^{13}C NMR (101 MHz, $CDCl_3$) δ 166.47, 158.30, 137.96, 130.58, 129.09, 124.75, 120.71, 118.97, 111.24, 55.58, 42.31, 41.30, 15.02, 13.49. Exact mass calcd for C14H19NO2 $[M+H]^+$: 234.1494; found 234.1500.

4.1.52. (E)-N-ethyl-3-(2-methoxyphenyl)acrylamide

6d was reacted with piperidine following the general procedure E to give the desired product **7k** as a light yellow powder (83.6%). ^{1}H NMR (400 MHz, $CDCl_3$) δ 7.85 (d, *J* = 15.8 Hz, 1H), 7.44 (dd, *J* = 7.6, 1.5 Hz, 1H), 7.32–7.26 (m, 1H), 6.90 (dd, *J* = 14.5, 7.8 Hz, 2H), 6.51 (d, *J* = 15.8 Hz, 1H), 5.85 (s, 1H), 3.85 (s, 3H), 3.48–3.36 (m, 2H), 1.19 (t, *J* = 7.3 Hz, 3H). ^{13}C NMR (101 MHz, $CDCl_3$) δ 166.60, 158.30, 136.16, 130.72, 129.02, 124.06, 121.97, 120.73, 111.20, 55.52, 34.66, 15.02. Exact mass calcd for C12H15NO2 $[M+H]^+$: 206.1181; found 206.1183.

*4.1.53. (E)-1-(piperidin-1-yl)-3-(thiophen-2-yl)prop-2-en-1-one (**7l**)*

6e was reacted with piperidine following the general procedure E to give the desired product **7l** as a light yellow powder (33.5%). ^{1}H NMR (400 MHz, $CDCl_3$) δ 7.78 (d, *J* = 14.9 Hz, 1H), 7.30 (d, *J* = 5.0 Hz, 1H), 7.20 (d, *J* = 3.5 Hz, 1H), 7.03 (dd, *J* = 5.0, 3.5 Hz, 1H), 6.72 (d, *J* = 14.9 Hz, 1H), 3.62 (s, 4H), 1.68 (d, *J* = 4.2 Hz, 2H), 1.62 (s, 4H). ^{13}C NMR (101 MHz, $CDCl_3$) δ 164.73, 138.77, 134.73, 130.07, 128.88, 127.32, 116.45, 46.97, 43.58, 26.21, 24.76. Exact mass calcd for C12H15NOS $[M+Na]^+$: 244.0772; found 244.0775.

*4.1.54. (E)-N,N-diethyl-3-(thiophen-2-yl)acrylamide (**7m**)*

6e was reacted with diethylamine following the general procedure E to give the desired product **7m** as a light yellow powder (41.5%). ^{1}H NMR (400 MHz, $CDCl_3$) δ 7.81 (d, *J* = 15.1 Hz, 1H), 7.29 (d, *J* = 5.1 Hz, 1H), 7.20 (d, *J* = 3.5 Hz, 1H), 7.02 (dd, *J* = 5.1, 3.5 Hz, 1H), 6.62 (d, *J* = 15.1 Hz, 1H), 3.55–3.37 (m, 4H), 1.21 (s, 6H). ^{13}C NMR (101 MHz, $CDCl_3$) δ 205.56, 165.53, 140.77, 135.17, 130.10, 128.08, 127.02, 116.75, 42.41, 41.23, 15.21, 13.35. Exact mass calcd for C11H15NOS $[M+Na]^+$: 232.0772; found 232.0774.

*4.1.55. (E)-N-ethyl-3-(thiophen-2-yl)acrylamide (**7n**)*

6e was reacted with ethylamine following the general procedure E to give the desired product **7n** as a light yellow powder (27.4%). ^{1}H NMR (400 MHz, $CDCl_3$) δ 7.73 (d, *J* = 15.3 Hz, 1H), 7.29 (d, *J* = 5.1 Hz, 1H), 7.19 (d, *J* = 3.4 Hz, 1H), 7.02 (dd, *J* = 5.1, 3.7 Hz, 1H), 6.19 (d, *J* = 15.3 Hz, 1H), 5.67 (s, 1H), 3.48–3.36 (m, 2H), 1.20 (t, *J* = 7.3 Hz, 3H). ^{13}C NMR (101 MHz, $CDCl_3$) δ 165.68, 140.18, 133.67, 130.24, 128.10, 127.23, 119.88, 34.75, 15.02. Exact mass calcd for C9H11NOS $[M+Na]^+$: 204.0459; found 204.0453.

4.2. Biological study

4.2.1. MTT assay

PC12 cells (1×10^4 cells/well) were seeded in 96-well plates for 24 h followed by pretreation with PIP analogues for another 24 h, and then replaced with fresh medium containing 650 μM H_2O_2. After 24 h exposing to H_2O_2, medium was replaced with fresh medium again. Cell viability was determined by MTT assay described as previously described [43].

4.2.2. Lactate dehydrogenase (LDH) release assay

PC12 cells (1×10^4 cells/well) were seeded in 96-well plates for 24 h followed by pretreated with different concentration PIP analogues (12.5, 25, 50 and 100 μM) for 24 h, and then replaced with fresh medium containing 650 μM H_2O_2. The content of LDH in the medium was measured using an LDH diagnostic kit (KeyGEN BioTECH, NanJing, Jiang Su, China) according to the instruction.

4.2.3. Apoptosis assay

PC12 cells (2×10^5 cells/well) were seeded into 6-well plates for 24 h followed by pretreation with different concentration PIP analogues (12.5, 25, 50 and 100 μM) for 24 h, and then replaced with fresh medium containing 650 μM H_2O_2. Apoptosis was detected using the Annexin V-FITC/PI Apoptosis Detection Kit (KeyGEN BioTECH, NanJing, Jiang Su, China) according to the manufacturer's instructions. Specifically, PC12 cells were harvested and washed with binding buffer, followed by Annexin V-FITC and Propidium iodide (PI) stained for 5 min and detected by flow cytometry (Beckman Coulter, Miami, FL, USA). Analysis was performed using Expo32 software (Beckman Coulter). Each sample was repeated three times.

4.2.4. Determination of intracellular ROS

ROS levels were monitored using the fluorescent probe 2′,7′-dichlorodihydrofluorescein diacetate (DCFH-DA). PC12 cells (1×10^4 cells/well) were seeded into 96-well plates. After pretreatment with **3b** (12.5, 25, 50 and 100 μM) for 24 h, the cells were induced with 300 μM of H_2O_2 for 24 h. At the end of induction,

PC12 cells were rinsed with serum-free medium and treated with DCFH-DA working solution (DCFH-DA: serum-free medium = 1:1000) for 15 min at room temperature in a dark environment. At the end of the incubation, extracellular DCFH-DA molecules were washed away using serum-free medium. Finally, fluorescence was detected using an inverted fluorescence microscope (Zeiss Axiovert 200, Shanghai, China) and Infinite M200 PRO Multimode Microplate (Tecan Group Ltd, Männedorf) (excitation 525 nm, emission 590 nm).

4.2.5. Measurement of mitochondrial membrane potential

JC-1 dye (KeyGEN BioTECH, NanJing, Jiang Su, China) was used to detect mitochondrial membrane potential of H_2O_2-induced PC12 cells. 4×10^5 cells/well were seeded into 24-well plates. After pretreatment with 3**b** (12.5, 25 and 50 μM) for 24 h, cells were induced with 650 μM H_2O_2 for 24 h. PC12 cells were then treated with pre-warmed JC-1 working solution (1:1000) for 20 min. After incubation, the cells were washed three times with Incubation Buffer (1:10). For signal quantification, the intensity of red fluorescence (excitation 525 nm, emission 590 nm) and green fluorescence (excitation 488 nm, emission 525 nm) was detected by Infinite M200 PRO Multimode Microplate (Tecan Group Ltd, Männedorf) and the depolarization of mitochondrial membrane potential was measured by the relative ratio of red fluorescence to green fluorescence signal. The fluorescent signal in the cells was also observed and recorded with an inverted fluorescent microscope (Zeiss Axiovert 200, Shanghai, China).

4.2.6. Western blot analysis

Western blotting was performed as previously described [25]. Cytoplasmic and nuclear proteins were prepared from PC12 cells using a nuclear and cytoplasmic protein extraction kit (KeyGEN BioTECH, NanJing, Jiang Su, China) according to the manufacturer's instructions. Equal amounts of protein samples were separated by denaturing SDS-PAGE, then transferred to PVDF membrane, and probed with antibody respectively. Band intensity was analyzed using Image Lab software (version 5.2.1, BIORAD, Hercules, USA).

4.2.7. Immunofluorescence assay

Immunofuorescence assay was used to evaluate the levels of Nrf2. Briefly, PC12 cells were seeds into slides after incubation with **3b** at a concentration of 25 μM for 0 h, 4 h, 6 h and 8 h. After treatment, the medium was aspirated and the cells were washed with PBS, fixed with cold methanol at −20 °C for 20 min, rinsed with PBST for 5 min. Fixed cells were incubated with anti-Nrf2 diluted 1:200 in 0.5% BSA (diluted by PBST) overnight. Fixed cells were incubated with anti-Nrf2 diluted 1:1000 in PBS overnight and washed and treated with Dylight 594-conjugated secondary antibody diluted 1:500 in 0.5% BSA for 1 h, and then nuclei were counterstained with 4′,6′-diamidino-2-phenylindole (DAPI). Subsequently, the cells were observed with a fuorescence microscope (Zeiss Axiovert 200, Shanghai, China).

4.2.8. ARE-luciferase activity assay

Human hepatoma HepG2 cells in 24-well plates were transfected with pGL3-ARE plasmid (gifted by professor Ling Wang, West China School of Pharmacy, Sichuan University) using Lipofectamine 2000 reagent at a ratio of 1:6 DNA/Lipofectamine and incubated in opti-MEM medium for 30 min at 37 °C, then DNA-lipid complex were added. After 6 h, cells were cultured in fresh medium. The cells were treated with different concentrations of **3b** after 48 h following the procedure described previously [44].

4.2.9. Knockdown of Nrf2 expression by shRNA transfection

The shRNAs targeting rat Nrf2 gene was used for Nrf2 knockdown experiments, and scrambled sequence (shNT) was used as a control. Exponentially growing cells were transfected with different shRNAs using GeneTran III transfection reagent according to the manufacture's instruction. After 48 h of transfection, the cells were cultured in DMEM containing 10% FBS, 2 mM glutamine, 100 units/mL penicillin/streptomycin at 37 °C in a humidified atmosphere of 5% CO_2 and selected by supplementation with 0.5 mg/mL of G418. Knockdown of the Nrf2 expression in the cells was analyzed by Western blotting.

4.2.10. Molecular docking

The Keap1 of *homo sapiens* has 624 residues. There are two main domains for the Keap1, one for BTB domain between 67 and 179 residue, the other one for Kelch domain with the 327–611 residue. There are many crystal structures for BTB or Kelch and no full length keap1 structure was available [9]. Hence, we selected the I-TASSER online service as the method to construct the homology structure for the full length Keap1. The 1U6D [45], 2DYH [46], 3HVE [47], 3I3N (Murray, unpublished), 3ZGD [48], 4AP2 [49] and 4IFJ (Pan, unpublished) were used as the temple models. The overall quality of the five homology models was verified by Verify 3D [50]. We selected the best one as our covalent docking homology model. The covalent docking was done with the AutoDock 4.2 using the two-point attractor and flexible side chain methods [51]. The side chain of Cys and the ligand molecule were flexibly. The binding grid box center was the C_α atom of Cys and the number points in X, Y and Z were 40 × 40 × 40 with 0.375 Å as the spacing. The ten conformation were identified by using a Lamarkian type of genetic algorithm for every covalent docking and selected the lowest estimated binding energy by the scoring function in the AutoDock 4.2.

4.2.11. Experiment animal and treatment

All animal experiments were performed according to the institutional guide for the care and use of laboratory animals, and all mouse protocols were approved by the Animal Care and Use Committee of Sichuan University Chengdu, Sichuan, China). Male 10-week-old C57BL/6 mice (weight, 20–23 g) were purchased from Dossy Experimental Animals Co. Ltd. (Chengdu, China). Food and water were given *ad libitum*, and mice were housed on a standard 12 h light/12 h dark cycle. Vehicle was treated with saline. In the prophylactic administration group, saline or **3b** (50 or 100 mg/kg) dissolved in the saline was orally administered for two weeks; on the third week, MPTP-HCl (25 mg/kg) or saline was intraperitoneally injected to create the MPTP-induced PD mouse models (n = 6 per group). In the therapeutic administration group, MPTP-HCl (25 mg/kg) or saline was intraperitoneally injected for one week to create the MPTP-induced PD mouse models and followed by saline or **3b** (100 mg/kg) dissolved in the saline was orally administered for two weeks (Fig. 7A). All mice were trained for pole and rotarod test in the last three days. Twenty-one days after treatment, the mice were sacrificed for further study.

4.2.12. Behavior tests

Behavior tests was performed to detected the motor ability. Pole and rotarod test were carried out as previously described [52].

4.2.13. Immunohistochemistry

Immunohistochemistry assays were performed to detect the expression of TH and Nrf2 in striatum and SNpc. These experiments were carried as previously described [53].

4.2.14. Statistical analysis

Data are reported as the mean ± SD. The significant difference between multiple treatments and the control was analyzed using a one-way ANOVA with Dunnett's post-test. *P* values less than 0.05

were considered statistically significant.

Declaration of competing interest

The authors declare that they have no known competing financial interests or personal relationships that could have appeared to influence the work reported in this paper.

Acknowledgement

The authors appreciate the financial support from the National Natural Science Foundation of China (81527806 and 81874297) and the 1.3.5 project for disciplines of excellence, West China Hospital, Sichuan University (ZY2017202).

Appendix A. Supplementary data

Supplementary data to this article can be found online at https://doi.org/10.1016/j.ejmech.2020.112385.

References

[1] L. Gan, M.R. Cookson, L. Petrucelli, A.R. La Spada, Converging pathways in neurodegeneration, from genetics to mechanisms, Nat. Neurosci. 21 (2018) 1300–1309.
[2] E.C. Hirsch, P. Jenner, S. Przedborski, Pathogenesis of Parkinson's disease, Movement disorders, Off. J. Mov. Disord. Soc. 28 (2013) 24–30.
[3] W.J. Herring, C. Assaid, K. Budd, R. Vargo, R.S. Mazenko, C. Lines, A. Ellenbogen, L. Verhagen Metman, A phase Ib randomized controlled study to evaluate the effectiveness of a single-dose of the NR2B selective *N*-methyl-D-aspartate antagonist MK-0657 on levodopa-induced dyskinesias and motor symptoms in patients with Parkinson disease, Clin. Neuropharmacol. 40 (2017) 255–260.
[4] W. Poewe, A. Antonini, Jan C.M. Zijlmans, Pierre R. Burkhard, F. Vingerhoets, Levodopa in the treatment of Parkinson's disease: an old drug still going strong, Clin. Interv. Aging 5 (2010) 229–238.
[5] P. Rizek, N. Kumar, M.S. Jog, An update on the diagnosis and treatment of Parkinson disease, Can. Med. Assoc. J. 188 (2016) 1157–1165.
[6] R. Pahwa, C.M. Tanner, R.A. Hauser, S.H. Isaacson, P.A. Nausieda, D.D. Truong, P. Agarwal, K.L. Hull, K.E. Lyons, R. Johnson, M.J. Stempien, ADS-5102 (amantadine) extended release capsules for levodopa-induced dyskinesia in Parkinson disease (EASE LID study): a randomized clinical trial, JAMA Neurol. 74 (2017) 941–949.
[7] A. Lloret-Villas, T.M. Varusai, N. Juty, C. Laibe, N. Le NovÈre, H. Hermjakob, V. Chelliah, The impact of mathematical modeling in understanding the mechanisms underlying neurodegeneration: evolving dimensions and future directions, CPT Pharmacometrics Syst. Pharmacol. 6 (2017) 73–86.
[8] G.H. Kim, J.E. Kim, S.J. Rhie, S. Yoon, The role of oxidative stress in neurodegenerative diseases, Exp. Neurobiol. 24 (2015) 325–340.
[9] Z.Y. Jiang, M.C. Lu, Q.D. You, Discovery and development of kelch-like ECH-associated protein 1. nuclear factor erythroid 2-related factor 2 (KEAP1:NRF2) protein-protein interaction inhibitors: achievements, challenges, and future directions, J. Med. Chem. 59 (2016) 10837–10858.
[10] D. Malhotra, E. Portales-Casamar, A. Singh, S. Srivastava, D. Arenillas, C. Happel, C. Shyr, N. Wakabayashi, T.W. Kensler, W.W. Wasserman, Global mapping of binding sites for Nrf2 identifies novel targets in cell survival response through ChIP-Seq profiling and network analysis, Nucleic Acids Res. 38 (2010) 5718–5734.
[11] T. Kensler, N.S. Wakabayashi, Cell survival responses to environmental stresses via the Keap1-Nrf2-ARE pathway, Annu. Rev. Pharmacol. Toxicol. 47 (2007) 89–116.
[12] M. Zhang, C. An, Y. Gao, R.K. Leak, J. Chen, F. Zhang, Emerging roles of Nrf2 and phase II antioxidant enzymes in neuroprotection, Prog. Neurobiol. 100 (2013) 30–47.
[13] S.J. Peng, B.X. Zhang, X.K. Meng, J. Yao, J.G. Fang, Synthesis of piperlongumine analogues and discovery of nuclear factor erythroid 2-related factor 2 (Nrf2) activators as potential neuroprotective agents, J. Med. Chem. 58 (2015) 5242–5255.
[14] A. Cuadrado, A.I. Rojo, G. Wells, J.D. Hayes, S.P. Cousin, W.L. Rumsey, A.T. Dinkova-Kostova, Therapeutic targeting of the NRF2 and KEAP1 partnership in chronic diseases, Nat. Rev. Drug Discov. 18 (2019) 295–317.
[15] M.S. Brennan, M.F. Matos, B. Li, X.P. Hronowski, B.B. Gao, P. Juhasz, J. Rhodes Kenneth, H. Scannevin Robert, Dimethyl fumarate and monoethyl fumarate exhibit differential effects on Keap1, Nrf2 activation, and glutathione depletion in vitro, PLoS One 10 (2015) 14.
[16] J. Wilson Anthony, K. Kerns Jeffrey, F. Callahan James, J. Moody Christopher, Keap calm, and carry on covalently, J. Med. Chem. 56 (2013) 7463–7476.
[17] Z. Lin, J.R. Hoult, D.C. Bennett, A. Raman, Stimulation of mouse melanocyte proliferation by Piper nigrum fruit extract and its main alkaloid, piperine, Planta Med. 65 (1999) 600–603.
[18] A. Sahebkar, Y. Henrotin, Analgesic efficacy and safety of curcuminoids in clinical practice: a systematic review and meta-analysis of randomized controlled trials, Pain Med. 23 (2015) 1192–1202.
[19] I. Bukhari, M. Alhumayyd, A. Mahesar, A. Gilani, The analgesic and anticonvulsant effects of piperine in mice, J. Physiol. Pharmacol. 64 (2013) 789–794.
[20] A. Yasir, S. Ishtiaq, M. Jahangir, M. Ajaib, K.M. Khan, Biology-oriented synthesis (BIOS) of piperine derivatives and their comparative analgesic and antiinflammatory activities, Med. Chem. 14 (2018) 269–280.
[21] Panahi, Y. Hosseini, M. Sadat, Khalili, Nahid, Naimi, Effat, Majeed, Muhammed, Antioxidant and anti-inflammatory effects of curcuminoid-piperine combination in subjects with metabolic syndrome: a randomized controlled trial and an updated meta-analysis, Clin. Nutr. 34 (2015) 1101–1108.
[22] X. Peng, T. Yang, G. Liu, H. Liu, Y. Peng, L. He, Piperine ameliorated lupus nephritis by targeting AMPK-mediated activation of NLRP3 inflammasome, Int. Immunopharmacol. 65 (2018) 448–457.
[23] C.D. Doucette, G. Rodgers, R.S. Liwski, D.W. Hoskin, Piperine from black pepper inhibits activation-induced proliferation and effector function of T lymphocytes, J. Cell. Biochem. 116 (2015) 2577–2588.
[24] S. Li, C. Wang, M. Wang, W. Li, K. Matsumoto, Y. Tang, Antidepressant like effects of piperine in chronic mild stress treated mice and its possible mechanisms, Life Sci. 80 (2007) 1373–1381.
[25] W. Yang, Y.H. Chen, H. Liu, H.D. Qu, Neuroprotective effects of piperine on the 1-methyl-4-phenyl-1,2,3,6-tetrahydropyridine-induced Parkinson's disease mouse model, Int. J. Mol. Med. 36 (2015) 1369–1376.
[26] A. Correia, A. Cruz, A. Aquino, J. Diniz, K. Santana, P. Cidade, J. Peixoto, D. Lucetti, M. Nobre, G. Cruz, Glauce Socorro de Barros Viana, Neuroprotective effects of piperine, an alkaloid from the Piper genus, on the Parkinson's disease model in rats, J. Neurol. Ther. 1 (2015) 1–8.
[27] X. Ning, Y. Guo, X. Wang, X. Ma, C. Tian, X. Shi, R. Zhu, C. Cheng, Y. Du, Z. Ma, Design, synthesis, and biological evaluation of (*E*)-3, 4-dihydroxystyryl aralkyl sulfones and sulfoxides as novel multifunctional neuroprotective agents, J. Med. Chem. 57 (2014) 4302–4312.
[28] A. Gomtsyan, Heterocycles in drugs and drug discovery, Chem. Heterocycl. Compd. 48 (2012) 7–10.
[29] B. Broughton Howard, A. Watson Ian, Selection of heterocycles for drug design, J. Mol. Graph. Model. 23 (2004) 51–58.
[30] H. Kubinyi, Drug research: myths, hype and reality, Nat. Rev. Drug Discov. 2 (2003) 665–668.
[31] Z. Rankovic, CNS physicochemical property space shaped by a diverse set of molecules with experimentally determined exposure in the mouse brain, J. Med. Chem. 60 (2017) 5943–5954.
[32] H. Rong, Y. Liang, Y. Niu, Rosmarinic acid attenuates β-amyloid-induced oxidative stress via Akt/GSK-3β/Fyn-mediated Nrf2 activation in PC12 cells, Free Radic. Biol. Med. 120 (2018) 114–123.
[33] P.R. Angelova, A.Y. Abramov, Role of mitochondrial ROS in the brain: from physiology to neurodegeneration, FEBS Lett. 592 (2018) 692–702.
[34] M.J. Valente, A.M. Araújo, R. Silva, L. Bastos Mde, F. Carvalho, P. Guedes de Pinho, M. Carvalho, 3,4-Methylenedioxypyrovalerone (MDPV): in vitro mechanisms of hepatotoxicity under normothermic and hyperthermic conditions, Arch. Toxicol. 90 (2016) 1959–1973.
[35] H.C. Bertrand, M. Schaap, L. Baird, N.D. Georgakopoulos, A. Fowkes, C. Thiollier, H. Kachi, A.T. Dinkova-Kostova, G. Wells, Design, synthesis, and evaluation of triazole derivatives that induce Nrf2 dependent gene products and inhibit the Keap1-Nrf2 protein-protein interaction, J. Med. Chem. 58 (2015) 7186–7194.
[36] M. Amadio, G. Scapagnini, S. Davinelli, V. Calabrese, S. Govoni, A. Pascale, Involvement of ELAV RNA-binding proteins in the post-transcriptional regulation of HO-1, Front. Cell. Neurosci. 8 (2015) 459.
[37] K. Heyninck, L. Sabbe, C.S. Chirumamilla, K. Szarc Vel Szic, P. Vander Veken, K.J.A. Lemmens, M. Lahtela-Kakkonen, S. Naulaerts, K. Op de Beeck, K. Laukens, G. Van Camp, A.R. Weseler, A. Bast, G.R.M.M. Haenen, G. Haegeman, W. Vanden Berghe, Withaferin a induces heme oxygenase (HO-1) expression in endothelial cells via activation of the Keap1/Nrf2 pathway, Biochem. Pharmacol. 109 (2016) 48–61.
[38] J. Yang, Y. Zhang, I-TASSER server: new development for protein structure and function predictions, Nucleic Acids Res. 43 (2015) W174–W181.
[39] G. Bianco, S. Forli, D.S. Goodsell, A.J. Olson, Covalent docking using autodock: two-point attractor and flexible side chain methods, Protein Sci. 25 (2016) 295–301.
[40] J. Wang, L. Huang, C. Cheng, G. Li, J. Xie, M. Shen, Q. Chen, W. Li, W. He, P. Qiu, Design, synthesis and biological evaluation of chalcone analogues with novel dual antioxidant mechanisms as potential anti-ischemic stroke agents, Acta Pharm. Sin. B 9 (2019) 335–350.
[41a] B.M. Choi, S.M. Kim, T.K. Park, G. Li, S.J. Hong, R. Park, H.T. Chung, B.R. Kim, Piperine protects cisplatin-induced apoptosis via heme oxygenase-1 induction in auditory cells, J. Nutr. Biochem. 18 (2007) 615–622;
[41b] N. Nandakumar, S. Muthuraman, P. Gopinath, P. Nithya, J. Gopas, R.S. Kumar, Synthesis of coumaperine derivatives: their NF-κB inhibitory effect, inhibition of cell migration and their cytotoxic activity, Eur. J. Med. Chem. 125 (2016) 1076–1087.
[42] D. Luo, H. Sharma, D. Yedlapudi, T. Antonio, M.E.A. Reith, A.K. Dutta, Novel multifunctional dopamine D_2/D_3 receptors agonists with potential neuroprotection and anti-alpha synuclein protein aggregation properties, Bioorg. Med. Chem. 24 (2016) 5088–5102.

[43] J. Yang, Y. Zhou, C. Xia, F. Yi, S. He, S. Li, H. Ye, C. Xie, W. Wu, C. Li, Isogambogenic acid induces apoptosis-independent autophagic cell death in human non-small-cell lung carcinoma cells, Sci. Rep. 5 (2015) 7697.
[44] Y. Yang, Y. Wang, T. Wang, X. Jiang, L. Wang, Screening active components of modified Xiaoyao powder as NRF2 agonists, Cell Biochem. Funct. 35 (2017) 518–526.
[45] X. Li, D. Zhang, M. Hannink, L.J. Beamer, Crystal structure of the Kelch domain of human Keap1, J. Biol. Chem. 279 (2004) 54750–54758.
[46] K.I. Tong, B. Padmanabhan, A. Kobayashi, C. Shang, Y. Hirotsu, S. Yokoyama, M. Yamamoto, Different electrostatic potentials define ETGE and DLG motifs as hinge and latch in oxidative stress response, Mol. Cell Biol. 27 (2007) 7511–7521.
[47] M. Zhuang, M.F. Calabrese, J. Liu, M.B. Waddell, A. Nourse, M. Hammel, D.J. Miller, H. Walden, D.M. Duda, S.N. Seyedin, T. Hoggard, J.W. Harper, K.P. White, B.A. Schulman, Structures of SPOP-substrate complexes: insights into molecular architectures of BTB-Cul3 ubiquitin ligases, Mol. Cell. 36 (2009) 39–50.
[48] S. Horer, D. Reinert, K. Ostmann, Y. Hoevels, H. Nar, Crystal-contact engineering to obtain a crystal form of the Kelch domain of human Keap1 suitable for ligand-soaking experiments, Acta Crystallogr. Sect. F Struct. Biol. Cryst. Commun. 69 (2013) 592–596.
[49] P. Canning, C.D. Cooper, T. Krojer, J.W. Murray, A.C. Pike, A. Chaikuad, T. Keates, C. Thangaratnarajah, V. Hojzan, V. Ayinampudi, B.D. Marsden, O. Gileadi, S. Knapp, F. von Delft, A.N. Bullock, Structural basis for Cul3 protein assembly with the BTB-Kelch family of E3 ubiquitin ligases, J. Biol. Chem. 288 (2013) 7803–7814.
[50] D. Eisenberg, R. Lüthy, J.U. Bowie, VERIFY3D: assessment of protein models with three-dimensional profiles, Methods Enzymol. 277 (1997) 396–404.
[51] G.M. Morris, R. Huey, W. Lindstrom, M.F. Sanner, R.K. Belew, D.S. Goodsell, A.J. Olson, Autodock4 and autodocktools4: automated docking with selective receptor flexibility, J. Comput. Chem. 30 (2009) 2785–2791.
[52] K. Matsuura, H. Kabuto, H. Makino, N. Ogawa, Pole test is a useful method for evaluating the mouse movement disorder caused by striatal dopamine depletion, J. Neurosci. Methods 73 (1997) 45–48.
[53] J.W. Choi, S. Kim, J.H. Park, H.J. Kim, S.J. Shin, J.W. Kim, S.Y. Woo, C. Lee, S.M. Han, J. Lee, A.N. Pae, G. Han, K.D. Park, Optimization of vinyl sulfone derivatives as potent nuclear factor erythroid 2-related factor 2 (Nrf2) activators for Parkinson's Disease therapy, J. Med. Chem. 62 (2019) 811–830.